

**BIOSYNTHESIS OF NOVEL MNO<sub>2</sub> NANOCAPSULES VIA C. SPINOSA  
EXTRACT AND HONEYBEE-DERIVED CHITOSAN: EXPLORING  
ANTIBACTERIAL AND ANTICANCER PROPERTIES**

Mohamed G. Elharrif <sup>a</sup>,

Nasser A. Hassan <sup>b</sup>,

Mohamed Sharaf <sup>c, d</sup>.

<sup>a</sup> Department of Basic Medical Sciences, College of Medicine, Shaqra University, Shaqra 11961, Saudi Arabia.

<sup>b</sup> Synthetic Unit, Department of Photochemistry, Chemical Industries Research Institute, National Research Centre, Cairo 12622, Egypt.

<sup>c</sup> Department of Biochemistry, Faculty of Agriculture, AL-Azhar University, Nasr City, Cairo 11651, Egypt.

<sup>d</sup> Department of Biochemistry and Molecular Biology, College of Marine Life Sciences, Ocean University of China, Qingdao, 266003, PR China.

**БИОСИНТЕЗ НОВЫХ НАНОКАПСУЛ MnO<sub>2</sub> С ПОМОЩЬЮ  
ЭКСТРАКТА C. SPINOSA И ХИТОЗАНА МЕДОНОСНОЙ ПЧЕЛЫ:  
ИЗУЧЕНИЕ АНТИБАКТЕРИАЛЬНЫХ И ПРОТИВОРАКОВЫХ  
СВОЙСТВ**

Мохамед Г. Эльхарриф <sup>1</sup>,

Насер А. Хасан <sup>2</sup>,

Мохамед Шараф <sup>3,4</sup>

<sup>1</sup> Кафедра фундаментальных медицинских наук, Медицинский колледж, Университет Шакры, Шакра 11961, Саудовская Аравия.

<sup>2</sup> Отдел синтеза, кафедра фотохимии, Научно-исследовательский институт химической промышленности, Национальный исследовательский центр, Каир 12622, Египет.

<sup>3</sup> Кафедра биохимии, факультет сельского хозяйства, Университет Аль-Азхар, Наср-Сити, Каир 11651, Египет.

<sup>4</sup> Кафедра биохимии и молекулярной биологии, Колледж наук о морской жизни, Океанский университет Китая, Циндао, 266003, Китайская Народная Республика.

## Abstract

This investigation delves into the integration of *Capparis spinosa* extract (CSLe) onto manganese dioxide nanoparticles ( $MnO_2$ NPs) and chitosan derived from honeybees (CSH) in a nanostructured configuration. The resultant nanocomposites, namely CSLe@ $MnO_2$ NPs and CSH/CSLe@ $MnO_2$ NPs, underwent thorough characterization through various analytical techniques. UV-Vis spectroscopy unveiled distinctive features, such as ligand-to-metal charge transfer and photoluminescence, affirming the successful chitosan-functionalization of the  $MnO_2$ NPs, thereby differentiating them from their pristine counterparts. FTIR spectra corroborated the binding of chitosan and identified crucial molecular functional groups. SEM-EDX analysis revealed the morphological properties, addressing non-uniform sizes in the as-calcined  $MnO_2$ NPs by the uniform coating of CSH on CSLe@ $MnO_2$ NPs, while EDX confirmed the presence of essential elements. TEM and SAED provided insights into the spherical morphology, crystalline structure, and lattice planes of these nanoparticles. Size distribution measurements highlighted distinctions between CSLe@ $MnO_2$ NPs and CSH/CSLe@ $MnO_2$ NPs. The nanomaterials underwent evaluation for their antimicrobial properties against a spectrum of Gram-negative and Gram-positive bacterial strains, with CSH/CSLe@ $MnO_2$ NPs exhibiting the highest bactericidal activity. Additionally, they demonstrated low minimum inhibitory concentration (MIC) values, especially against *S. aureus* (MIC as low as 12.5  $\mu$ g/ml). Their efficacy extended to anti-biofilm formation, significantly diminishing biofilm development in a dose-dependent manner, a pivotal factor in addressing biofilm-related infections. The study also scrutinized their cytotoxicity against normal Vero and PC<sub>3</sub> prostate cancer cells, revealing potential anticancer properties. Dose-dependent reductions in cell viability were observed for both normal and cancer cells. In conclusion, these findings underscore the versatility and promise of CSH/CSLe@ $MnO_2$ NPs in diverse biomedical applications, including antibacterial, anti-biofilm, and anticancer therapies.

**Keywords:** *C. spinosa*,  $MnO_2$ NPs, Honeybees chitosan, Antibacterial, Anti-biofilm, Anticancer.

## Резюме

Настоящее исследование посвящено описанию нанесения экстракта *Carpathis spinosa* (CSLE) на наночастицы диоксида марганца ( $MnO_2NP$ ) и хитозан медоносных пчел (CSH) в наноструктурированной конфигурации.

Полученные нанокомпозиты, а именно CSLE@ $MnO_2NPS$  и CSH/CSLE@ $MnO_2NPS$ , были тщательно охарактеризованы с помощью различных аналитических методов. спектроскопия в УФ- и видимой области обнаружила отличительные особенности, такие как перенос заряда «лиганд-металл» и фотолюминесценцию, подтверждая успешную функционализацию хитозана на  $MnO_2NP$ , тем самым дифференцируя их от соответствующих интактных аналогов. Спектры инфракрасной спектроскопии с преобразованием Фурье (ИКФС) подтвердили связывание хитозана и идентифицировали ключевые молекулярные функциональные группы.

Анализ с помощью способа линейного сканирования SEM-EDX выявил морфологические свойства, касающиеся неравномерных размеров в as-calcined  $MnO_2NP$  с помощью равномерного покрытия CSH на CSLE@ $MnO_2NP$ , в то время как энергодисперсионный рентгеноспектральный микроанализ (EDX) подтвердил наличие необходимых элементов. Просвечивающая электронная микроскопия (TEM) и электронная дифракция на отдельных участках (SAED) дали представление о сферической морфологии, кристаллической структуре и плоскости кристаллической таких наночастиц. Измерения распределения по размерам выявили различия между CSLe@ $MnO_2NPs$  и CSH/CSLe@ $MnO_2NPs$ .

Нanomатериалы прошли оценку на антимикробные свойства в отношении различных грамотрицательных и грамположительных бактериальных штаммов, с максимальной бактерицидной активностью у CSH/CSLe@ $MnO_2NPs$ . Кроме того, минимальная ингибирующая концентрация (MIC), особенно против *S. aureus* (MIC не более 12,5 мкг/мл)

описана при низких значениях. Их эффективность также распространялась на формирование антибиопленки, достоверно дозозависимо снижая образование биопленки как ключевого фактора в отношении инфекций, связанных с биопленкой. Также тщательно изучена цитотоксичность соединений в отношении нормальных клеток Vero и клеток рака предстательной железы РСЗ, выявившая дозозависимое снижение жизнеспособности клеток обеих линий. В заключение, полученные результаты подчеркивают универсальность и перспективность CSH/CSLE@MNO<sub>2</sub>NP в различных биомедицинских целях, включая антибактериальные, подавление синтеза антибиопленки и противоопухолевую терапию.

**Ключевые слова:** *C. spinosa*, Mno<sub>2</sub>nps, хитозан медоносной пчелы, антибактериальные, антибиопленка, противораковые.

## 1 **1 Introduction**

2 Nanotechnology has significantly transformed the medical landscape, providing  
3 innovative solutions to a myriad of healthcare challenges. Manganese dioxide  
4 nanoparticles ( $MnO_2$ NPs) have garnered substantial attention owing to their unique  
5 properties and promising applications in medicine [1].  $MnO_2$ NPs, acting as carriers  
6 for therapeutic drugs, facilitate targeted drug delivery to specific cells or tissues,  
7 thereby minimizing side effects and amplifying the therapeutic efficacy of  
8 medications. The functionalization of  $MnO_2$ NPs allows for controlled drug release  
9 at the desired location, making them indispensable for personalized medicine and  
10 improved treatment outcomes [2].

11 In the context of healthcare,  $MnO_2$ NPs possess diverse pharmacological properties  
12 that render them invaluable for medical applications. These properties encompass  
13 antioxidant, antimicrobial, neuroprotective, anticancer, and wound-healing  
14 attributes. The multifaceted pharmacological profile of  $MnO_2$ NPs positions them  
15 as promising agents in disease treatment and healthcare, playing a pivotal role in  
16 reshaping medical treatments, offering innovative solutions across a spectrum of  
17 diseases, and enhancing patient outcomes [3, 4].

18 Chitosan, a biopolymer derived from chitin found in the shells of crustaceans like  
19 shrimp and crabs, is a remarkably versatile material. Particularly intriguing is its  
20 utilization when sourced from honeybee exoskeletons in a nanostructured form, a  
21 relatively novel and less-explored avenue[5]. Bee-derived chitosan boasts  
22 intriguing pharmacological properties with potential applications across various  
23 medical and pharmaceutical contexts[6]. It exhibits biocompatibility and  
24 biodegradability, making it ideal for drug encapsulation and controlled release,  
25 particularly in targeted cancer therapy. Chitosan nanoparticles can target specific  
26 tissues or cells, enhancing drug absorption while minimizing side effects.  
27 Additionally, its antimicrobial properties make it effective against bacteria and

28 fungi, useful in wound healing and medical device coatings. Chitosan's ability to  
29 form gels and films also supports tissue engineering and regeneration. [7,8].

30 *Capparis spinosa*, commonly known as caper, has been utilized in traditional  
31 medicine for centuries due to its rich phytochemical composition and diverse  
32 pharmacological properties. Key compounds like quercetin, rutin, catechin, and  
33 various flavonoids contribute to its therapeutic potential, offering antioxidant, anti-  
34 inflammatory, antimicrobial, and potentially anti-diabetic benefits. This botanical  
35 extract shows promise in managing conditions such as arthritis, inflammatory  
36 bowel diseases, and combating microbial infections, while also potentially  
37 regulating blood sugar levels. [9,10]

38 Incorporating *C. spinosa* into nanostructures presents a promising avenue for  
39 enhancing its pharmacological properties. Nanostructured drug delivery systems  
40 can significantly improve the bioavailability and therapeutic efficacy of its  
41 bioactive compounds. By encapsulating phytochemicals in nanoparticles or  
42 nanocarriers, these formulations enhance solubility, enable controlled and  
43 sustained release, and target specific cells or tissues, thereby optimizing  
44 therapeutic impact while minimizing side effects. This modern approach holds  
45 potential for making *C. spinosa* more effective and efficient in various therapeutic  
46 applications. [11,12]

47 Furthermore, Nanoencapsulation of *C. spinosa's* bioactive compounds safeguards  
48 them from degradation, boosting stability and shelf life, vital for herbal medicine  
49 efficacy. Recent studies have effectively encapsulated these compounds into  
50 nanostructures like liposomes and nanoparticles, enhancing pharmacokinetic and  
51 pharmacodynamic properties [13]. This advancement in nanomedicine offers  
52 promising avenues for improving *C. spinosa's* therapeutic potential, paving the  
53 way for enhanced drug development and natural product-based therapies [14].



54 Precise targeting of therapies remains a challenge despite the potential of  
55 nanostructures for targeted drug delivery. Understanding their interaction with  
56 specific cells or tissues is essential. Moreover, comprehensive studies on the long-  
57 term effects and potential toxicity of these materials are lacking. Ensuring the  
58 biocompatibility and biodegradability of nanostructures is crucial for their safe  
59 application in medical treatments. Therefore, the primary goal of this study is to  
60 assess the antibacterial and anticancer properties of Manganese Dioxide (MnO<sub>2</sub>)  
61 combined with extracts from the *C. spinosa* plant, incorporated into nanoparticles  
62 and mixed with honeybee-derived chitosan. This innovative combination is being  
63 investigated as a potential new pharmacologically active compound. Additionally,  
64 we aim to identify and characterize the nanoparticles used in this formulation. This  
65 research endeavors to shed light on the potential therapeutic applications of these  
66 compounds, addressing both their antimicrobial and anticancer effects

## 67 **2 Material and methods**

### 68 ***2.1. Plant collection and preparation***

69 *C. spinosa*, samples were collected from habitats at northwestern coastal region  
70 (Alex-Marsa Matrouh Road, 62Km west of El-Hammam city), at the recorded site  
71 30 44 46.88828°N, 29 12 8.0926 °E, the collected samples were identified  
72 authenticated taxonomically by the Herbarium, at Desert Research Center, Cairo,  
73 Egypt. *C. spinosa*, samples were washed by distilled water then were shade dried  
74 at lab-temperature till constant weight. Then, grounded into fine powdery form,  
75 sieved and finally stored in dry glass jar at room temperature for further use.

### 76 ***2.2. Extraction of natural molecules of C. spinosa, samples***

77 *C. spinosa* were dried at 60 °C till a constant dry weight and ground to powder.  
78 Then, 10 g of *C. spinosa*, powder was added to a conical flask with a 100 ml  
79 capacity, 5 ml of 2% phenol water, and 10 ml of 30% trichloroacetic acid. After

80 shaking the mixture and letting it sit for a whole night, the filtrate was created up  
81 to 50 ml [15].

### 82 **2.3. HPLC**

83 *C. spinosa*, sample were subjected to identification of phenolic compounds using  
84 HPLC. 10 µl of the sample was injection and analyzed at flow rate 0.7 mL/min  
85 using Agilent 1200 LC–MS–ESI instrument (positive mode) with a diode array  
86 detector set at 254, 280, 320 and 520 nm. Agilent Zorbax Eclipse plus C18 column  
87 using nitrogen as nebulizing gas was used. Mobil phase used was 1% formic acid  
88 (A) and acetonitrile (B); gradient was 0 min 5 % B, 1 min 20 % B, 6 min 20 % B,  
89 8 min 80 % B, 18 min 80 % B, 19 min 5 % B and 20 min 5 % . Mass scanned in  
90 the range m/e 0-1000 at fragmentation energy 20 eV and potential 4.0 kV [16].

### 91 **2.4. Chitosan bee's extraction**

92 Several phases were involved in the extraction of biopolymers of chitin and  
93 chitosan from a novel potential source which dead corniolan honeybees hybrid  
94 were collected in front of bee hives during the autumn season 2022 from the  
95 commercial apiary located in Motobes region Kafr El-Sheikh Governorate, Egypt.  
96 To extract chitin, the protein (deproteination) and mineral (demineralization)  
97 elements of subpestilence are first dissolved and removed. The raw honey bee *Apis*  
98 *mellifera* material was first ground using (CM 190 Cemotec TM, Denmark).  
99 Demineralization was then performed using the Hackman technique with minor  
100 modifications [17], by treating the crushed raw material with 2 M hydrochloric  
101 acid (ratio,1:10 ) for 5 h at 25–27 °C. Then, deproteination was accomplished by  
102 treating the pulverized raw materials with a 1 N sodium hydroxide solution for 1 h  
103 at a temperature of 80–85°C. Then, dried at 60–65 °C for 4h.

### 104 **2.5. Preparation of CSLe@MnO<sub>2</sub>NPs, and CSH/CSLe@MnO<sub>2</sub>NPs**

105 Co-precipitation and green chemistry methods were used to synthesize MnO<sub>2</sub>NPs.  
106 To this end, 0.47 g KMnO<sub>4</sub> precursor was dissolved in 20 ml of deionized water.  
107 *C. spinosa* extract was then added drop by drop to the previous solution and stirred

108 at 40 °C for 2 h using a magnetic stirrer. The resultant solution was dried in an  
109 oven at 80 °C. The powder obtained was calcined at 400 °C for 2 h. For extracted  
110 chitosan from dead bees (CHN) solutions was prepared by dissolving 1 g of  
111 chitosan in 100 mL of 1.0% aqueous acetic acid and stirring until the liquid  
112 became translucent. Then, the CSLe@MnO<sub>2</sub>NPs were combined by ionic gelation  
113 process with the create bees chitosan. Finally, the suspension was stirred under  
114 magnetic stirring at room temperature and left to qualify for 30 min. The bee  
115 chitosan NPs were then centrifuged at 3000 rmb for 15 min at 3-5 °C and freeze-  
116 dried with 10% (m/m) trehalose in a Freeze-dryer for 24 h [18].

## 117 **2.6. Characterization of prepared samples**

118 A PerkinElmer Spectrum 100 Fourier transform infrared (FTIR) spectrometer  
119 (PerkinElmer, MA) with an attenuated total reflection (ATR) accessory of  
120 germanium crystal with a high-resolution index (4.0), performing 64 scans for each  
121 spectrum at 4 cm<sup>-1</sup> resolution, was used to collect the FTIR spectra of  
122 CSLe@MnO<sub>2</sub>NPs, and CSH/CSLe@MnO<sub>2</sub>NPs samples in the 500–4000 cm<sup>-1</sup>  
123 range. [19]. By applying 10 µl of diluted material to holey carbon films on copper  
124 grids, TEM was utilized to examine the shape and distribution of the MnO<sub>2</sub> NPs,  
125 and CSH/CSLe@MnO<sub>2</sub>NPs. The samples were seen functioning at a 200 kV  
126 accelerating voltage. ImageJ software, version 1.52a, was used to measure  
127 nanoparticle size. SEM with EDX analysis (Tescan Vega3, Czechia) was  
128 performed at scale levels of 20 µm, 2 µm, 1 µm and 500 nm with the magnification  
129 of 1000×, 10,000× and 50,000×. ImageJ software was applied to calculate  
130 crystallite size from 2D SEM images. X-ray diffraction (JEOL JDX-3623, Japan)  
131 analysis was performed with CuKα (wavelength = 1.5418 Å) radiation from 2θ  
132 values of 10° to 80° with applied current and voltage range of 2.5-30 mA and 20-  
133 40 kV, respectively [20].

## 134 **2.7. Bacterial sample collection**

135 All the isolated Gram-positive bacteria *Staphylococcus aureus*, *Staphylococcus*  
136 *hominis*, and *Enterococcus faecalis*, Gram-negative bacteria *Escherichia coli*,  
137 *Klebsiella pneumonia* and *Acinetobacter baumannii* were collected from the  
138 Microbiology Department, Faculty of Medicine, Cairo University, Egypt, through  
139 the proper protocol and identified and diagnosed based on morphological  
140 characteristics and biochemical examinations according to the standard methods of  
141 diagnosis and confirmed with the Vitek 2 compact [21, 22]

#### 142 **2.8. Determination of minimum inhibitory concentration (MICs) and minimum** 143 **bactericidal concentration (MBCs)**

144 By using the usual dilution approach, a broth micro dilution assay was used to  
145 estimate the MIC of antibacterial activity in 96 multi-well micro titer plates (CLSI  
146 M07-A8). 100 µl of TSB (Himedia) were dispersed evenly across all wells. A  
147 volume of 100 µl from each CSLe, CSLe@MnO<sub>2</sub>NPs, and CSH/CSLe@MnO<sub>2</sub>NPs  
148 (10<sup>24</sup> - 2.5 µg mL<sup>-1</sup>) were pipetted into the wells of the first row of the micro titer  
149 plate. Finally, 100 µl of freshly made, 0.5 McFarland matching turbid bacterial  
150 solution were put to each well. Each plate contained two columns that served as  
151 both positive and negative controls. Wrapped plates were incubated for 18–24 h at  
152 37°C. The plates were visually inspected for the presence or absence of turbidity  
153 against a dark background. The MIC was determined as the lowest concentration at  
154 which there was no discernible bacterial growth when compared to controls.  
155 Additionally, stock inoculum suspensions were made in trek diagnostic systems  
156 sterile saline with 1% tween 80 from 7days colonies on potato dextrose agar slants  
157 (provided by Remel, Lenexa, Kans) used to estimate the MIC of antifungal  
158 activities. A 95% of the stock inoculum suspensions measured 0.9 × 10<sup>6</sup> to 4.5 ×  
159 10<sup>6</sup> CFU/mL. On test day, each microdilution well was infected with 100 µl of the  
160 diluted (Twofold) conidial inoculum suspensions in liquid potato. Then, 200 µl per  
161 well of Dextrose Agar (PDA) and microdilution trays were tested after 4 days at  
162 28°C. The MICs goals were the lowest CSLe, CSLe@MnO<sub>2</sub>NPs, and

163 CSH/CSLe@MnO<sub>2</sub>NPs concentrations that inhibited growth completely (100%  
164 inhibition). By sub culturing 20µl from the clear wells of the MICs and MBCs was  
165 ascertained.

## 166 **2.9. Anti-biofilm viability assay**

167 The crystal violet staining test was determined the impact of CSLe,  
168 CSLe@MnO<sub>2</sub>NPs, and CSH/CSLe@MnO<sub>2</sub>NPs on biofilm formation by *S. aureus*,  
169 *S. haemolyticus*, *E. faecalis*, *A. baumannii*, *K. pneumoniae*, and *E. coli* [23, 24].

170 In brief, 20 µl of each isolated bacteria was added overnight to growth. Different  
171 concentrations of CSLe, CSLe@MnO<sub>2</sub>NPs, and CSH/CSLe@MnO<sub>2</sub>NPs (1.562  
172 and 25 mg/mL) were added to 180 µL of LB medium with 0.2% (w/v) glucose and  
173 incubated at 30 °C for 24 h. Then, washing with phosphate buffer pH7.4 got rid of  
174 the planktonic cells, and a 0.1% crystal violet solution was used to color the  
175 biofilm that stuck to the surface. After 15 min, sterile-distilled water was used to  
176 wash the crystal violet that had been taken apart. Last, the crystal violet that was  
177 stuck to the biofilm was released with 200 µl of 95% ethanol. The intensity of the  
178 crystal violet at 570 nm was measured with a UV–vis spectrophotometer.

$$179 \quad \% \text{ Biofilm formation} = (\text{OD control} - \text{OD sample}) / (\text{OD control}) \times 100$$

180 (1)

## 181 **2.10. Evaluation of cytotoxicity by MTT Assay**

182 Both control CSLe, CSLe@MnO<sub>2</sub>NPs, and CSH/CSLe@MnO<sub>2</sub>NPs conjugates  
183 were subjected to cytotoxicity evaluation by MTT assay. For this purpose, Vero  
184 ATCC CCL-81 normal cells and PC3 prostate cancer cell line were used to assess  
185 the anticancer potential, as reported by [25, 26]. Briefly, Vero ATCC CCL-81 and  
186 PC<sub>3</sub> cells were grown for 24 h at 37 °C in 96-well microtiter plates (pre-inoculated  
187 with MnO<sub>2</sub>NPs alone, and CSH/CSLe@MnO<sub>2</sub>NPs conjugates) using a DMEM that  
188 was additionally supplemented with 10% of FBS. After 24 h incubation, the

189 DMEM was removed. The Vero ATCC CCL-81 and PC<sub>3</sub> cells were again  
190 incubated for 4 h at 37 °C in the presence of 20 µL of MTT (5 mg/mL in PBS)  
191 supplemented fresh medium. Following that, DMSO (150 µL/well) was used to  
192 solubilize the formazan crystals resulting from the mitochondrial reduction of  
193 MTT. Finally, the absorbance was recorded at 570 nm (2300 EnSpire Multilabel  
194 Plate Reader, Perkin Elmer).

195 The OD should be directly interrelated to the quantity of cellular activity.

196 % Cell viability = (OD test – OD blank)/(OD control – OD blank)

197 (2)

198 , where OD optical density, test indicates the cells exposed to the CSLe,  
199 CSLe@MnO<sub>2</sub>NPs, and CSH/CSLe@MnO<sub>2</sub>NPs sample, control in term the control  
200 sample, and blank in term the wells without Vero ATCC CCL-81cercopithecus  
201 aethiops kidney normal cells and PC<sub>3</sub> prostate cancer cell lines.

## 202 **2.11. Statistics analysis**

203 Data was presented as mean ± standard error of mean. GraphPad prism software  
204 program (version 7.0 (2016) Inc., San Diego, CA, USA) was applied in statistical  
205 analysis. The statistical difference among groups was examined by one-way  
206 ANOVA subsequently Post hoc-Tukey's test for comparison between groups. All  
207 *p* values (\**P*<0.05, \*\**P*<0.01, \*\*\**P*<0.001and \*\*\*\**P*<0.0001), were regarded as  
208 statistically significant. [27, 28].

## 209 **3 Results**

### 210 **3.1. HPLC**

211 The HPLC retention durations of the phytoconstituents were compared to the  
212 retention periods of the used reference samples to confirm their identities. Four  
213 compounds were found in the aqueous extract of the *C. spinosa* after HPLC  
214 analysis. Some identification was on the basis of evaluations against current  
215 criteria. The substances that were found all products of nature, two compounds of

216 phenolic acids, one compound of each glycoside, and hydroxybenzoate as shown  
217 in Fig 1. 19 chemical compounds were identified and purified using HPLC. The  
218 percentages of the detected chemicals were computed and compared to the total  
219 peaks in the HPLC chromatogram, showing that naringenin (flavonoid),  
220 vanillin(organic compound), chlorogenic acid (polyphenol), daidzein (isoflavone),  
221 ferulic acid (polyphenol), and methyl gallate (*gallate* ester) were the major  
222 isolated compounds at a concentration of 22.41%, 14.05%, 13.97%, 9.59%,9.45%  
223 and 5.71% respectively. Furthermore the result showed catechin (flavan-3-ol) at a  
224 concentration of 2.72%, gallic acid (phenolic acids) at a concentration of 2.89 %,  
225 coffeic acid (phenolic acids) at a concentration of 3.40%, querectin (flavonol) at a  
226 concentration of 0.527%, syringic acid (phenolic acids) at a concentration of  
227 0.250%, rutin (flavonoid) at a concentration of 0.0559 %, cinnamic acid (organic  
228 compound) at a concentration of 0.0584% and hesperetin (flavonoid) at a  
229 concentration of 0.0626 % .

### 230 **3.2. Characterization of CSLe@MnO<sub>2</sub>NPs, and CSH/CSLe@MnO<sub>2</sub>NPs**

#### 231 **3.2.1. UV–vis spectroscopic**

232 The UV-visible spectroscopic analysis (Fig. 2A) were demonstrated the presence  
233 of ligand-to-metal charge transfer from chitosan to Mn<sup>2+</sup> ions in the MnO<sub>2</sub>NPs.  
234 Additionally, the room temperature photoluminescence exhibited many distinct  
235 characteristics, which are not often seen in unmodified MnO<sub>2</sub>NPs. The  
236 determination and quantification of the production of chitosan, CSLe@MnO<sub>2</sub>NPs,  
237 and CSH/CSLe@MnO<sub>2</sub>NPs were conducted utilizing the intensity of UV-Vis  
238 absorption peaks. Fig. 2A illustrates the presence of a large absorption peak at  
239 wavelengths of 350 nm, 245 nm, and 250 nm, respectively.

#### 240 **3.2.2. FTIR spectra**

241 The ligands were generated and the molecules and functional groups were  
242 identified by the acquisition of FTIR spectra for the as-calcined MnO<sub>2</sub>NPs



243 nanoparticles, CSLe plant, and the composite of MnO<sub>2</sub> NPs with Hypericum. The  
244 findings are shown in Fig. 2B. The vibrational modes associated with Mn-O-Mn  
245 interactions are responsible for the absorption peaks seen within the wavenumber  
246 range of 550–650 cm<sup>-1</sup>. The presence of covalent bonding between the ligand  
247 chitosan and the CSLe@MnO<sub>2</sub>NPs was verified by the observed alteration in the  
248 FTIR spectra, namely in the region associated with the stretching of C-N bonds at  
249 a wavenumber of 1210 cm<sup>-1</sup>. The existence of C-O aromatic carbon compounds is  
250 indicated by the absorption peak seen at 1300 cm<sup>-1</sup> in the combination of CSLe  
251 plant and NPs. Furthermore, the presence of CO-O-CO stretching vibrations may  
252 be detected by the emergence of a peak at 1050 cm<sup>-1</sup> and surface OH groups at  
253 3330 cm<sup>-1</sup> in the CSLe and CSLe@MnO<sub>2</sub>NPs, as seen in Fig. 2B.

### 254 3.2.3. SEM- EDX

255 In order to investigate the morphological characteristics of the SCLe@MnO<sub>2</sub>NPs,  
256 scanning electron microscopy (SEM-EDX) was used. As shown in Fig. 2C, the  
257 SEM picture revealed that the SCLe@MnO<sub>2</sub> NPs, which were subjected to  
258 calcination, exhibited diameters ranging from 22 to 35 nm, as indicated in the  
259 inset. The mean size of the NPs is determined to be around 25 nm. It is important  
260 to acknowledge that the SCLe@MnO<sub>2</sub>NPs exhibit heterogeneity and non-  
261 uniformity across various regions as a result of adhesion and agglomeration  
262 phenomena. The phenomenon described may be attributed to the process of  
263 calcination and subsequent exposure to high temperatures, resulting in the  
264 agglomeration of nanoparticles due to their inclination to minimize energy. Fig. 2D  
265 displays a scanning electron microscopy (SEM) picture of the composite material  
266 consisting of SCLe@MnO<sub>2</sub>NPs incorporated with chitosan. The homogenous  
267 coating of CSH on the surface of CSLe@MnO<sub>2</sub>NPs is evident, indicating the  
268 effective attachment of CSH to the composite. This may be attributed to the larger  
269 size and less agglomeration of the resultant composite compared to  
270 SCLe@MnO<sub>2</sub>NPs. In addition, the energy-dispersive X-ray (EDX) spectra of



271 manganese dioxide nanoparticles reveals the presence of oxygen and manganese,  
272 with corresponding weight percentages of 40.21% and 60.89%. The provided data  
273 illustrates a prominent peak seen at an energy level of 0.2688 kiloelectron volts  
274 (keV), which is indicative of the presence of a manganese-oxygen (Mn-O) bond.  
275 The presence of elemental peaks of manganese and oxygen in the data supports the  
276 conclusion that the production of CSLe@MnO<sub>2</sub>NPs has occurred, as seen in Figure  
277 2E. The composition of the shown elements includes oxygen (11.82%), carbon  
278 (21.39%), gold (12.67%), and manganese (54.12%). The findings presented in this  
279 study provide confirmation of the successful production of a nanocomposite  
280 material consisting of chitosan on CSLe@MnO<sub>2</sub>NPs. The low proportion of  
281 manganese concentration in the nanocomposite might likely be attributed to the  
282 inclusion of manganese dioxide nanoparticles inside the internal porous structure  
283 of the chitosan support, as seen in Fig. 2F.

#### 284 **3.2.4. TEM (HRTEM) images and selected area electron diffraction (SAED)**

285 In contrast, Fig.3 illustrates the TEM images of the as-calcined CSLe@MnO<sub>2</sub>NPs  
286 and composited CSH/CSLe@MnO<sub>2</sub>NPs. The TEM images demonstrates that the  
287 CSLe@MnO<sub>2</sub>NPs have a shape resembling spheres (Fig. 3A). Furthermore, the  
288 TEM examination provides further confirmation of the observed accumulation of  
289 CSH/CSLe@MnO<sub>2</sub>NPs and the subsequent increase in their dimensions (Fig. 3B).  
290 The interfering distance of the high-resolution transmission electron microscopy  
291 (HRTEM) was measured to be 0.49 nm, indicating the presence of the (101) plane  
292 in the crystal lattice of CSLe@MnO<sub>2</sub>NPs (refer to Fig. 3C). Additionally, the  
293 interfering distance was found to be 0.65 nm, corresponding to the (211) plane of  
294 the CSH/CSLe@MnO<sub>2</sub>NPs crystal lattice (refer to Fig. 3D).The transmission  
295 electron micrographs (TEM) reveal the presence of spherical morphology and  
296 uniform dispersion of CSLe@MnO<sub>2</sub> nanoparticles. The electron diffraction pattern  
297 obtained from the selected area electron diffraction (SAED) technique exhibits  
298 diffraction rings that may be attributed to the (101) and (200) crystallographic

299 planes, as seen in Fig 3E. The diffraction rings shown in Fig. 3F correspond to the  
300 (211) planes, which provide evidence for the presence of the spinel hausmannite  
301 structure in the SCH/CSLe@MnO<sub>2</sub> NPs. Moreover, the size distribution of NPs  
302 were determined and shown in Fig. 3G and H. The experimental findings  
303 demonstrated that the CSLe@MnO<sub>2</sub>NPs composite exhibited a particle size of  
304 25.27 nm, as shown in Fig. 3G. Additionally, the CSH/CSLe@MnO<sub>2</sub>NPs  
305 composite displayed a particle size of 98.87 nm, as illustrated in Fig. 3H.

### 306 **3.3. Antimicrobial activity by agar well diffusion assay and MICs and MBC** 307 **assays**

308 The antibacterial potentialities of pristine CSLe, CSLe@MnO<sub>2</sub>NPs, and  
309 CSH/CSLe@MnO<sub>2</sub>NPs conjugates were evaluated against the bacterial strains of  
310 Gram-negative (*A. baumannii*, *K. pneumoniae* and *E. coli*) and Gram-positive (*S.*  
311 *aureus*, *S. haemolyticus*, and *E. faecalis*) compared to leaves extract of CSLe. The  
312 results obtained are listed in Table 1 and shown in Fig. 4. After incubation period,  
313 CSLe were found to be bactericidal up to a certain extent against all the tested  
314 strains. CSLe were displayed lowest inhibition zone of 21mm of *E. coli* and the  
315 largest inhibition zone of 29 mm of *S. aureus*. However, the experimental results  
316 showed that the CSLe@MnO<sub>2</sub> NPs are good antibacterial agents. The lowest zones  
317 of inhibition have been found as 25 mm for *K. pneumoniae*, and the largest  
318 inhibition zone of 31 mm of *S. aureus* and *E. faecalis*. Furthermore, the optimally  
319 yielded CSH/CSLe@MnO<sub>2</sub> NPs conjugate was found to be highly bactericidal  
320 against all test strains. As shown in Fig. 4, zone value reduction from 33 mm  
321 against *S. haemolyticus* and 31mm against *A. baumannii* was recorded.

322 The broth dilution technique was used to determine the bacteriostatic effects of  
323 SCLe, SCLe@MnO<sub>2</sub>NPs, and CSH/SCLe@MnO<sub>2</sub>NPs against various harmful  
324 bacteria. As shown in Table 2, SCLe, and SCLe@MnO<sub>2</sub>NPs showed antimicrobial  
325 against Gram-negative and Gram-positive bacteria. At low concentrations,  
326 However, coated CSH onto SCLe@MnO<sub>2</sub>NPs were increased the activity

327 significantly. In contrast, the MIC results revealed that CSH/SCLe@MnO<sub>2</sub>NPs  
328 were more potent against Gram-negative bacteria than other nanosubstances. The  
329 results showed that MIC of the SCLe@MnO<sub>2</sub>NPs for the selected Gram-positive  
330 bacterial isolates was 12.5 µg/ml of *S. aureus*. While the visual turbidity test  
331 showed that CSH/SCLe@MnO<sub>2</sub>NPs inhibited *E. coli* and *K. pneumonia strains*  
332 (12.5 µg mL<sup>-1</sup>) was close to the standard antibiotic gentamicin control inhibition  
333 effectiveness varied (8 µg mL<sup>-1</sup>)

### 334 **,3.6.2. Anti-Biofilm Formation**

335 After 24 h treatment and incubation, our findings indicate that the application of  
336 SCLe, SCLe@MnO<sub>2</sub>NPs, and CSH/SCLe@MnO<sub>2</sub>NPs at sub-inhibitory  
337 concentrations resulted in a significant decrease in the formation of individual  
338 bacterial biofilms, as shown by the observed reduction in OD<sub>570</sub> nm values. The  
339 production of biofilms by *S. aureus*, *S. haemolyticus*, *E. faecalis*, *A. baumannii*, *K.*  
340 *pneumoniae*, and *E. coli* was shown to decrease in a way that was dependent on the  
341 dosage of SCLe, SCLe@MnO<sub>2</sub>NPs, and CSH/SCLe@MnO<sub>2</sub>NPs, as depicted in  
342 [Figs.5A, B, and C](#). In comparison to the control group, the use of SCLe resulted in  
343 a significant decrease in biofilm formation. The greatest inhibitory effect was seen  
344 with *S. aureus* bacteria, showing an inhibition rate of around 73.62%. However,  
345 the percentage of inhibition was somewhat lower when SCLe was associated with  
346 *A. baumannii*, at approximately 73.95% ([Fig. 5A](#)). In addition, the experimental  
347 investigation involving the application of nano-samples SCLe@MnO<sub>2</sub>NPs and  
348 CSH/SCLe@MnO<sub>2</sub>NPs for the treatment of biofilms revealed noteworthy  
349 outcomes. Specifically, the analysis indicated that the bacteria *S. aureus* exhibited  
350 the highest inhibition percentage, with rates of approximately 88.89% and 91.16%  
351 for SCLe@MnO<sub>2</sub>NPs and CSH/SCLe@MnO<sub>2</sub>NPs, respectively. Conversely, the  
352 bacteria *K. pneumonia* demonstrated the lowest inhibition percentage, with rates of  
353 about 79.28% and 89.62% for SCLe@MnO<sub>2</sub>NPs and CSH/SCLe@MnO<sub>2</sub>NPs,  
354 respectively (refer to [Figs. 5B and C](#)). The quantity of biofilm that developed in

355 the presence of these organisms was contrasted with the quantity of biofilm that  
356 formed in their absence. That is, without the use of SCLe, SCLe@MnO<sub>2</sub>NPs, and  
357 CSH/SCLe@MnO<sub>2</sub>NPs. Hence, it can be inferred that the use of chitosan-coated  
358 SCLe@MnO<sub>2</sub>NPs has promise as a viable therapeutic approach for the  
359 management of bacterial infections and perhaps other ailments connected with  
360 biofilm formation.

### 361 *3.5. Cytotoxicity against and morphological features of normal Vero ATCC* 362 *CCL-81 and PC<sub>3</sub> prostate cancer cells*

363 The literature extensively documents the cytotoxicity of pure metal nanoparticles  
364 derived from various sources. Nevertheless, there is a lack of available data  
365 regarding the cytotoxicity of MnO<sub>2</sub>NPs synthesized using green methods,  
366 specifically utilizing leaf extracts from *C. spinosa* and conjugating them with bee  
367 chitosan. This cytotoxicity assessment is intended to be conducted on Vero ATCC  
368 CCL-81 cells and the PC<sub>3</sub> prostate cancer cell line. These nanoparticles have  
369 significant potential for various biomedical applications, particularly in combating  
370 human carcinoma. To bolster the comprehensiveness of our research, we  
371 undertook an inquiry into the cytotoxic properties and anticancer potential of  
372 SCLe, SCLe@MnO<sub>2</sub>NPs, and CSH/SCLe@MnO<sub>2</sub>NPs conjugates. The  
373 investigation was conducted on Vero cells, which are considered normal, and PC<sub>3</sub>  
374 prostate cancer cells. The Vero cells and PC<sub>3</sub> cancer cells were cultivated in 96-  
375 well microtiter plates at a temperature of 37 °C in the presence of each SCLe,  
376 SCLe@MnO<sub>2</sub>NPs, and CSH/SCLe@MnO<sub>2</sub>NPs. Three replicates were performed  
377 for each concentration, and an untreated control sample was included in the  
378 experiment. The toxicological impact was quantified by evaluating the extent of  
379 growth suppression shown by the SCLe, MnO<sub>2</sub>NPs, and CSH/SCLe@ MnO<sub>2</sub>NPs  
380 in relation to the control group, which showed a growth rate of 100%. [Fig.6](#)  
381 illustrates the cytotoxic characteristics of the chemicals under investigation, as  
382 represented by the percentage of cellular viability.

383 The optimally generated CSH/SCLe@MnO<sub>2</sub>NPs conjugates showed decreased cell  
384 viability in Vero cells and PC<sub>3</sub> malignant cells as compared to the control sample.  
385 It was shown that this decrease in cell viability was dose-dependent, with a 50%  
386 inhibitory concentration (IC<sub>50</sub>). Furthermore, it was noted that 48 h of incubation  
387 were required for the IC<sub>50</sub> of the evaluated SCLe, SCLe@MnO<sub>2</sub>NPs, and  
388 CSH/SCLe@MnO<sub>2</sub>NPs conjugates against Vero cells and PC<sub>3</sub> cancer cells. The  
389 CSH/SCLe@MnO<sub>2</sub> nanoparticle conjugates may have anticancer effects, as shown  
390 by the observed inhibitory concentration and rate of cell death/viability. At high  
391 doses (250 µg mL<sup>-1</sup>), a considerable amount of cytotoxicity (83.38%) was detected  
392 when Vero cells were exposed to CSH/SCLe@MnO<sub>2</sub>NPs. It was found that the  
393 IC<sub>50</sub> values for this therapy were 116.11±3.36 µg mL<sup>-1</sup>. Comparatively, at the  
394 same concentrations, the cytotoxicity of SCLe and MnO<sub>2</sub>NPs alone produced  
395 lower levels of cytotoxicity (49.68% and 51.54%, respectively). The results  
396 showed that the IC<sub>50</sub> values for SCLe and SCLe@MnO<sub>2</sub>NPs alone were 2252.01 ±  
397 4.14 µg mL<sup>-1</sup> and 245.35 ± 4.9 µg mL<sup>-1</sup>, in that order (Fig. 6A). Moreover, at high  
398 doses of 250 µg/mL<sup>-1</sup>, PC<sub>3</sub> cells treated with CSH/SCLe@MnO<sub>2</sub>NPs showed a  
399 69.39% cytotoxic impact. The treatment's IC<sub>50</sub> values were found to be 205.25 ±  
400 2.53 µg mL<sup>-1</sup>. By contrast, at the same doses, SCLe and SCLe@MnO<sub>2</sub>NPs alone  
401 demonstrated cytotoxicity of 55.20% and 64.44%, respectively. The results  
402 showed that the IC<sub>50</sub> values for SCLe and SCLe@MnO<sub>2</sub>NPs were 236.84 ± 8.58  
403 µg mL<sup>-1</sup> and 213.11 ± 3.96 µg mL<sup>-1</sup>, respectively. Data shown in Fig. 6B.

### 404 **3.6. Morphological features**

405 The morphological properties of PC<sub>3</sub> cancer cell lines, untreated normal Vero cell  
406 lines, and cell lines treated with different dosages of SCLe, MnO<sub>2</sub>NPs, and  
407 CSH/SCLe@MnO<sub>2</sub>NPs are all reported and compared in this work. The  
408 absorbance values acquired from the 3T3 Phototox program were used to  
409 determine the amounts of prepared samples in various cell lines. Following the red  
410 dye's capture and accounting for the amounts of SCLe, MnO<sub>2</sub>NPs, and

411 CSH/SCLe@ MnO<sub>2</sub>NPs used in the viability assays, these absorbance values were  
412 determined (Figs. 6C and D).

#### 413 4 Discussion

414 The demand for environmentally friendly synthesis methods for nanoparticles has  
415 surged, driven by the widespread use of metal-based nanomaterials in diverse  
416 sectors, including industry, medicine, and environmental applications [29]. In  
417 recent years, there has been a growing emphasis on harnessing the potential of  
418 herbal medicines, abundant in diverse phytometabolites, for the eco-friendly  
419 synthesis of nanoparticles. This approach shows promise in combating bacterial  
420 infections and contributing to cancer prevention[30].Consequently, we utilized *C.*  
421 *spinosa* for the synthesis of MnO<sub>2</sub> NPs. Through HPLC, we identified and purified  
422 19 chemical compounds. Environmental factors, such as temperature, soil  
423 composition, water availability, and humidity, have been shown to impact plant  
424 growth, the production of secondary metabolites, and biological activities,  
425 potentially reflected in the HPLC results [31]. In our research, we examined the  
426 enhanced antibacterial, antibiofilm, and anticancer properties of CSLe when  
427 employed in the biofabrication of MnO<sub>2</sub>NPs. Importantly, the resulting  
428 CSLe@MnO<sub>2</sub>NPs did not exhibit cytotoxic effects. Despite using identical source  
429 materials, variations in surface composition, aggregation patterns, and nanoparticle  
430 sizes gave rise to differences in observed biological activities and NPs related  
431 cytotoxicity [32]. The formation of the absorption peak at 350 nm indicated the  
432 presence of MnO<sub>2</sub>NPs [30]. The intensity of absorption peaks at the same  
433 wavelength (350 nm) was used to measure the NPs yield. The peak at 350 nm is  
434 due to d–d electron transitions of Mn<sup>4+</sup> ions in MnO<sub>2</sub>NPs [33]. Surface  
435 functionalizing ligands, nanoparticle size, and surface charge represent three  
436 critical determinants influencing the precise distribution of nanomaterials within  
437 living organisms. In this context, we have modified CSLe@MnO<sub>2</sub>NPs by  
438 introducing a biocompatible ligand, chitosan, owing to its established capacity to



439 selectively target and adhere to the outer membrane of bacteria. This strategic  
440 modification is expected to enhance the penetration of MnO<sub>2</sub>NPs and their  
441 interaction with cellular organelles within microbial cells. [31, 32]. According to  
442 our findings, FTIR spectra of SCLe, CSLe@MnO<sub>2</sub>NPs and CSH/SCLe@  
443 MnO<sub>2</sub>NPs exhibited absorption peaks similar with previous report[34].  
444 Furthermore, TEM and SEM results showed that the particle size of clearly in  
445 CSH/SCLe@ MnO<sub>2</sub>NPs greater than CSLe@MnO<sub>2</sub>NPs which indicates that the  
446 addition of CSH increased the size of the SCLe@ MnO<sub>2</sub>NPs and the particals size  
447 dispersion was in the desired range of reported nano [35, 36]. These observations  
448 deviated somewhat from the findings of Fabre et al. 2020 [37], where they  
449 observed that unloaded nanoparticles were smaller in size than loaded  
450 nanoparticles. The characteristics identified in the EDX analysis align with prior  
451 research studies.[32, 38, 39].

452 Our HPLC analysis revealed that the plant extract is rich in phenolic compounds,  
453 flavonoids, and terpenoids, known for their active antimicrobial and anti-biofilm  
454 properties[40, 41]. Phenolic compounds play a pivotal role in biofilm formation at  
455 the cellular level by inducing several significant changes. These changes involve  
456 altering the stiffness of the cell wall, increasing the permeability of the cell  
457 membrane, and influencing various intracellular processes. These effects occur  
458 primarily through the formation of hydrogen bonds between phenolic compounds  
459 and enzymes within the cell. This interaction can disrupt the structural integrity of  
460 the cell wall, compromise the integrity of the cell membrane, and interfere with  
461 essential cellular processes [42]. Consistent with our findings, numerous well-  
462 regarded studies have extensively examined the correlation between the  
463 antibacterial effectiveness of flavonoids and their structural characteristics.  
464 Additionally, several research groups have elucidated the antibacterial mechanisms  
465 of specific flavonoids. For instance, the antibacterial activity of quercetin has been  
466 attributed to its ability to inhibit DNA gyrase, a critical enzyme involved in

467 bacterial DNA replication and repair processes [43]. Moreover, in a separate study  
468 involving different flavonoids tested against various strains of *K. pneumoniae*, all  
469 flavonoids demonstrated antimicrobial activity comparable to the standard  
470 antibacterial agent ofloxacin. This underscores the potential of flavonoids as  
471 effective antimicrobial agents and highlights the diversity of their antibacterial  
472 mechanisms[44].

473 On the other hand, metal oxide nanoparticles, including copper oxide (CuO),  
474 manganese oxide (MnO), zinc oxide (ZnO), nickel oxide (NiO), magnesium oxide  
475 (MgO), iron oxide (FeO), ferric oxide ( $Fe_2O_3$ ), and chromium oxide ( $Cr_2O_3$ ),  
476 among others, have garnered significant attention and exploration for various  
477 biological applications. These nanoparticles have been extensively studied for their  
478 potential in antibacterial, antibiofilm, and anticancer application[45]. Metal oxide  
479 nanoparticles exhibit unique properties that make them suitable for a wide range of  
480 biological uses. Their antimicrobial properties can help combat bacterial and  
481 fungal infections. Our antimicrobial findings align with previous studies by  
482 Manjula et al.[46, 47] and Kunkalekar et al. [48], which also observed a stronger  
483 inhibitory effect of Manganese dioxide ( $MnO_2$ ) nanoparticles against Gram-  
484 positive bacteria compared to Gram-negative bacteria. This discrepancy in  
485 effectiveness might be attributed to diverse mechanisms at play, such as DNA  
486 damage and disruption of the bacterial cell membrane.  $MnO_2$  NPs have  
487 demonstrated a differential impact on Gram-positive and Gram-negative bacteria  
488 due to variations in their cell wall structures. The rigid peptidoglycan layer in  
489 Gram-positive bacteria makes them more susceptible to damage, including DNA  
490 strand breakage, induced by the oxidative stress generated by  $MnO_2$  NPs. In  
491 contrast, the outer membrane of Gram-negative bacteria, composed of  
492 lipopolysaccharides, provides a protective barrier against some nanoparticles,  
493 making them comparatively more resilient [49]. The antibacterial efficacy of  
494 CSLe@ $MnO_2$  NPs can be attributed to their relatively small size, facilitating their



495 penetration into bacterial cells, and subsequent disruption of the cell membranes.  
496 The small size of these nanoparticles allows them to infiltrate the bacterial cells  
497 effectively, where they interact with the cell membrane. As a result of this  
498 interaction, the cell membrane integrity is compromised, leading to structural  
499 damage and permeability changes. These alterations create an environment where  
500 vital cellular processes are disrupted, eventually culminating in the demise of the  
501 bacterial cell [50]. In a study conducted by Khan et al. [51], they successfully  
502 synthesized MnO NPs through the utilization of *A. indicum*, followed by an  
503 assessment of the green-synthesized AI-MnONPs. Interestingly, the AI-MnONPs  
504 demonstrated a notably high and comparable antibacterial effectiveness against *B.*  
505 *subtilis* and *S. aureus* when compared to conventional antibiotic drugs. This  
506 enhanced antibacterial impact could be attributed to a variety of factors,  
507 particularly the influence of the nanoparticle structure and composition on key  
508 bacterial cell membrane properties. [52, 53]. In addition, a study by Muhamed et  
509 al. 2018 [54], manganese oxide nanoparticles were synthesized using lemon extract  
510 and curcumin extract. The research yielded compelling results, indicating that  
511 MnO NPs modified with curcumin and aniline exhibited superior antibacterial  
512 effectiveness. These modified MnONPs demonstrated a remarkable capability to  
513 prevent the growth of various bacterial pathogens, including *S. aureus*, *B. subtilis*,  
514 *S. typhusa* as well as fungal strains like *C. albicans*, *C. lunata*, and *T. simii* [55, 56].  
515 In 2015, Azhir and colleagues synthesized manganese trioxide (Mn<sub>3</sub>O<sub>4</sub>)  
516 nanoparticles using the precipitation method. These Mn<sub>3</sub>O<sub>4</sub> NPs exhibited robust  
517 antimicrobial activity against bacterial pathogens, specifically *E. coli* and *S.*  
518 *aureus*. Notably, when evaluating the antibacterial characteristics of these  
519 nanoparticles, a noteworthy observation emerged: *E. coli* displayed a higher degree  
520 of sensitivity to Mn<sub>3</sub>O<sub>4</sub> NPs in comparison to Gram-positive bacteria like *S.*  
521 *aureus*. This discrepancy in response may be attributed to variations in the  
522 structural composition of bacterial cell walls. [57]. In a separate study, Joshi et al.  
523 in 2020 successfully synthesized manganese dioxide nanoparticles, which

524 exhibited notable antimicrobial activity against a range of bacteria, including *S.*  
525 *aureus*, *P. vulgaris*, *S. typhi*, *S. mutants*, and *E. coli* [49]. Likewise, Kumar et al.  
526 conducted experiments wherein Mn<sub>3</sub>O<sub>4</sub> nanoparticles were prepared at various pH  
527 levels, and their antimicrobial properties were assessed using the disk diffusion  
528 method. Their findings indicated that these nanoparticles exhibited stronger  
529 antibacterial effects against Gram-negative bacteria compared to Gram-positive  
530 ones [58]. This differential response is attributed to the presence of negative charge  
531 domains on the cell walls of both Gram-positive and Gram-negative bacteria.  
532 However, Mn<sub>3</sub>O<sub>4</sub> nanoparticles are able to penetrate the outer membrane and  
533 interact with the underlying cell wall and membrane components [59].  
534 Our hypothesis revolves around the idea that the increased alkalinity of chitosan-  
535 coated SCLe@MnO<sub>2</sub>NPs may be attributed to the presence of negatively charged  
536 domains on bacterial cell walls. This negative charge is believed to play a  
537 significant role in how chitosan-coated SCLe@MnO<sub>2</sub>NPs interact with bacterial  
538 cell walls, primarily through electrostatic forces or coordination-derived forces.  
539 Additionally, it's important to note that metallic nanoparticles often carry a positive  
540 charge on their surface, which can further contribute to their ability to disrupt  
541 bacterial cell walls and enhance the permeability of nanoparticles into the cells.  
542 [60, 61].

543 The broth dilution technique employed to assess the bacteriostatic effects of SCLe,  
544 SCLe@MnO<sub>2</sub>NPs, and CSH/SCLe@MnO<sub>2</sub>NPs against a range of pathogenic  
545 bacteria [62]. Notably, the heightened antibacterial effectiveness of  
546 CSH/CSLe@MnO<sub>2</sub>NPs can be attributed to a synergistic interplay between the  
547 physical characteristics of the nanoparticles and the adsorption of bioactive  
548 phytomolecules from the leaves extract of *C. spinosa* onto their surface [63]. These  
549 results also highlighted that the synthesized CSH/CSLe@MnO<sub>2</sub>NPs displayed  
550 greater activity against Gram-positive bacteria in contrast to their efficacy against  
551 Gram-negative bacterial species. This differential response is likely linked to the  
552 structural and compositional differences between the cell walls of Gram-negative

553 and Gram-positive bacterial strains[46]. Nanopolymers, particularly nanochitosan,  
554 have been extensively investigated due to their unique bioactivity and their utility  
555 as carriers for drug delivery, as well as their antimicrobial, antitumor, and gene  
556 delivery capabilities, either in isolation or in combination with other active  
557 compounds [64, 65]. Numerous prior studies have also reported similar findings,  
558 highlighting the greater efficacy of unmodified chitosan against Gram-negative  
559 bacterial strains compared to Gram-positive ones [66-69]

560 Numerous research studies have revealed the presence of various anticancer  
561 mechanisms linked to chitosan-based nanoparticles. These nanoparticles have  
562 exhibited substantial effectiveness in suppressing the proliferation of human  
563 carcinoma cell lines in in vitro experiments. [70-72]. In our study, we conducted an  
564 evaluation of SCLe, SCLe@MnO<sub>2</sub>NPs, and CSH/SCLe@MnO<sub>2</sub>NPs in vitro  
565 against both normal and cancer cell lines. We aimed to assess their impact on cell  
566 morphology and potential cytotoxic effects. To do this, we utilized 3T3 Phototox  
567 software to observe identifiable morphological features associated with apoptosis  
568 after exposing normal Vero ATCC CCL-81 and PC<sub>3</sub> prostate cancer cell lines to  
569 these samples for 24 h. The results of this evaluation revealed concentration-  
570 dependent morphological changes in the cells, particularly evident in the  
571 concentration range of 250 to 500  $\mu\text{g mL}^{-1}$ . Notably, the enhanced  
572 cytotoxicity observed with CSH/SCLe@MnO<sub>2</sub>NPs can be linked to an increase in  
573 the generation of hydrogen peroxide (H<sub>2</sub>O<sub>2</sub>). This heightened H<sub>2</sub>O<sub>2</sub> production  
574 follows the conversion of SCLe crude extract into highly reactive superoxide or  
575 hydroxyl radicals. [73]. Furthermore, the antioxidant properties and protective  
576 effects of the plant extracts can be attributed to the presence of total phenolic, total  
577 flavonoid, total saponins, and total alkaloids content in SCLe. These compounds  
578 are capable of scavenging free radicals, reducing reactive oxygen species (ROS),  
579 and thereby minimizing oxidative stress. Additionally, these phytochemical  
580 substances can influence intracellular redox processes and the balance of ROS,

581 leading to the conversion of ROS into highly reactive superoxide or hydroxyl  
582 radicals, subsequently resulting in oxidative stress. [74, 75]. This oxidative stress  
583 can lead to various cellular outcomes, including apoptosis, DNA damage,  
584 cytotoxicity, and disruptions in cell signaling, [76]. Importantly, after 24 h of  
585 incubation with the various cell lines, no discernible cytotoxicity or intracellular  
586 ROS generation was observed in any of the samples at doses up to 250 µg mL<sup>-1</sup>.  
587 These findings suggest that chitosan-based nanoparticles may hold significant  
588 potential as therapeutic agents for the treatment of human carcinoma. Their  
589 selective cytotoxicity towards cancer cells while sparing normal cells makes them  
590 promising candidates for further development as anticancer treatments.

## 591 **5 Conclusion**

592 In conclusion, this study has successfully developed a straightforward and cost-  
593 effective method for synthesizing MnO<sub>2</sub>NPs utilizing leaf extracts from *C. spinosa*.  
594 The nanoparticles underwent thorough characterization, resulting in the synthesis  
595 of CSLe@MnO<sub>2</sub>NPs and CSH/CSLe@MnO<sub>2</sub>NPs. These nanomaterials exhibited  
596 distinctive features, including ligand-to-metal charge transfer and  
597 photoluminescence. The introduction of chitosan coating led to more uniform  
598 particle sizes. Significantly, these nanomaterials demonstrated potent antibacterial  
599 properties against a broad spectrum of bacterial strains, with  
600 CSH/CSLe@MnO<sub>2</sub>NPs displaying exceptional efficacy. They also exhibited low  
601 MIC values, particularly against *S. aureus*. Additionally, the nanomaterials  
602 showcased notable anti-biofilm capabilities in a dose-dependent manner,  
603 addressing the challenge of biofilm-related infections. Cytotoxicity assessments  
604 underscored their potential in anticancer applications, with dose-dependent  
605 reductions in cell viability observed in both normal and cancer cells. This  
606 comprehensive study highlights the versatility and promise of  
607 CSH/CSLe@MnO<sub>2</sub>NPs across various biomedical applications, presenting exciting

608 prospects for future research and advancements in the fields of nanomedicine and  
609 biotechnology.

### 610 **Aacknowledgements**

611 The author extend their appreciation to the deanship of scientific research at  
612 Shaqra University for funding this research work through the project number (SU-  
613 ANN-2023059)

### 614 **Declarations**

615 Ethics approval

616 The research protocol was reviewed and approved by the ethics committee of the  
617 Shaqra University, Saudi Arabia (approval number: ERC\_SU\_20230033) and all  
618 procedures were carried out in accordance with the applicable rules and  
619 regulations. The study was carried out in accordance with ARRIVE guidelines.

### 620 **Competing interests**

621 There are no declared conflicts of interest for the authors.

**ТАБЛИЦЫ**

**Table 1.** Zone diameter (mm) interpretative standards chart and tested samples for the disc diffusion method of determining antimicrobial sensitivity and resistance status of common human bacterial pathogens .

N o.	Isolate Name	Antibacterial activity (mm)				
		-ve	+ve	SCL e	SCLe @MnO <sub>2</sub> NPs	SCH/SCLe@Mn O <sub>2</sub> NPs
1	<i>Staphylococcus aureus</i>	0	25	29	31	34
2	<i>Staphylococcus haemolyticus</i>	0	21	23	29	33
3	<i>Enterococcus faecalis</i>	0	22	27	31	35
4	<i>Acinetobacter baumannii</i>	0	20	22	24	31
5	<i>Klebsiella pneumoniae</i>	0	20	22	25	33
6	<i>Escherichia coli</i>	0	22	21	26	33

**Table 2.** MIC determinations of the NPs against fungal and bacterial human

Tested microorganisms	Samples					
	SCLe mg/ml		SCLe@MnO <sub>2</sub> NPs μg/ml		CSH/SCLe@MnO <sub>2</sub> NPs μg/ml.	
	MICs	MBCs	MICs	MBCs	MICs	MBCs
Gram positive bacteria						
<i>E. faecalis</i>	25	100	25	50	50	100
<i>S. aureus</i>	50	100	12.5	25	50	100
<i>S. hominis</i>	50	100	25	50	50	100
Gram negative bacteria						
<i>E. coli</i>	50	100	50	50	12.5	25
<i>K. pneumonia</i>	50	100	50	50	12.5	25
<i>A. baumannii</i>	25	100	50	50	25	50

pathogens micro-strains.

## РИСУНКИ

**Figure 1.** HPLC chromatogram of *C. spinosa* extract.

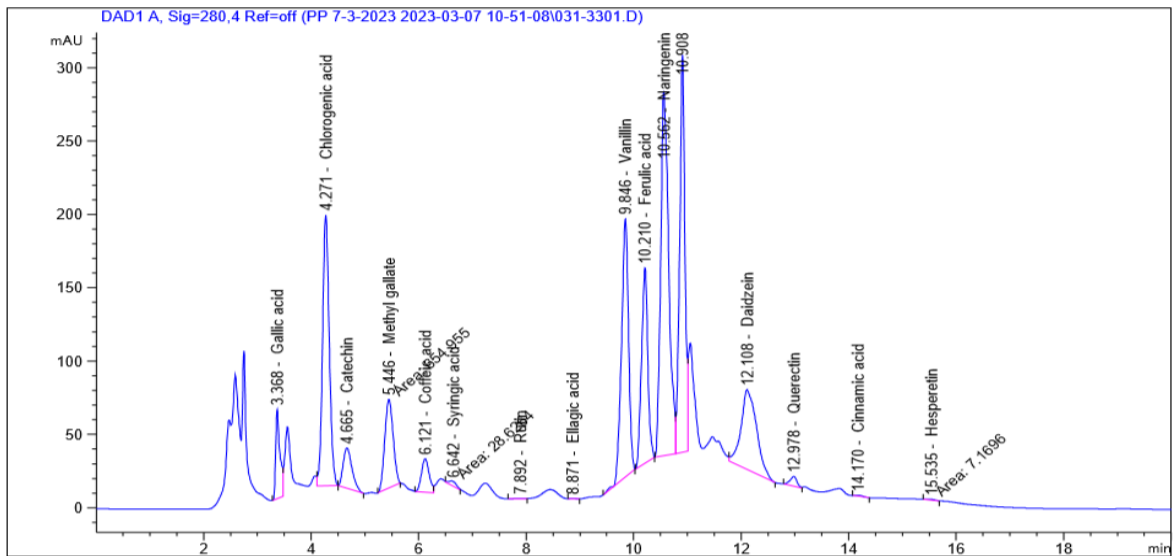




**Figure 2.** Physico-chemical characterization (A) UV–vis spectroscopic, (B) FTIR of CSH, CSLe@MnO<sub>2</sub>NPs, and CSH/CSLe@MnO<sub>2</sub>NPs, (C and D) SEM image (magnification 5 μm and 200nm), and (E and F) EDX microphotographs of CSLe@MnO<sub>2</sub>NPs, and CSH/CSLe@MnO<sub>2</sub>NPs composite.

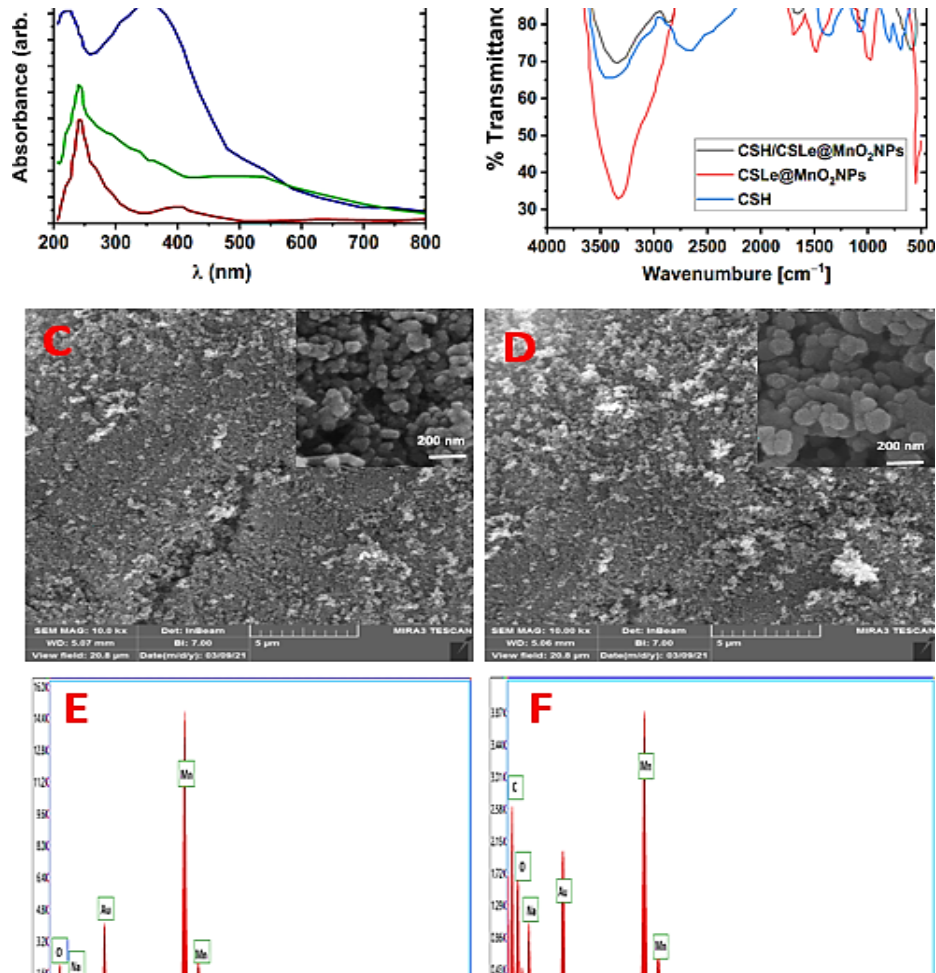


**Figure 3.** Physico-chemical characterization (A and B) TEM image. (C and D) High-resolution TEM (HRTEM) image and (E and F) SAED pattern of the same. of a single nanoparticle. (G and H) Size distribution measured by TEM of CSLe@MnO<sub>2</sub>NPs, and CSH/CSLe@MnO<sub>2</sub>NPs composite.

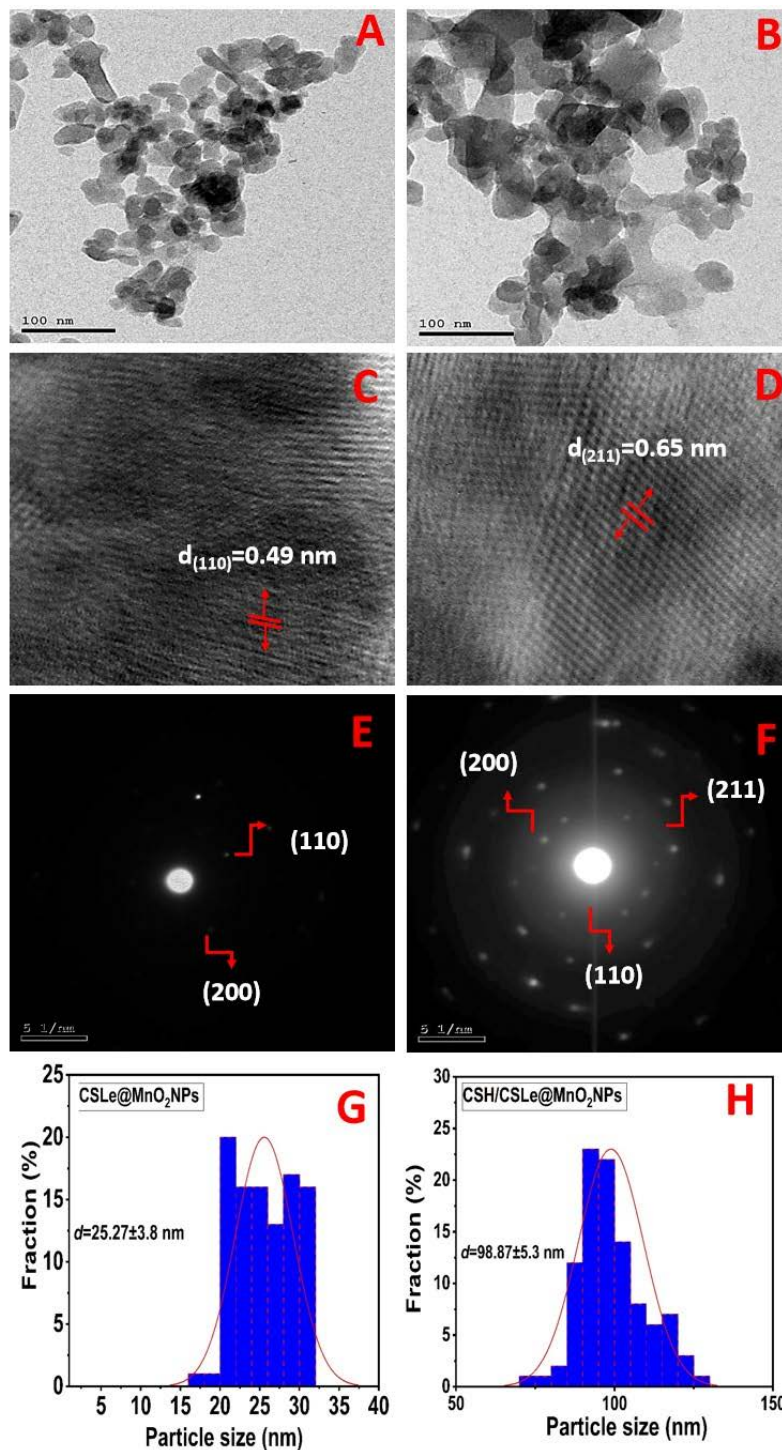


**Figure 4.** The inhibition zone of different pathogenic bacteria strains *S. aureus*, *S. hominis*, *E. faecalis*, *A. baumannii*, *K. pneumoniae*, and *E. coli* against by (A) Negative control (dH<sub>2</sub>O), (B) positive control, (C) SCLe, (D) SCLe@MnO<sub>2</sub>NPs, and (E) CSH/SCLe@MnO<sub>2</sub>NPs.

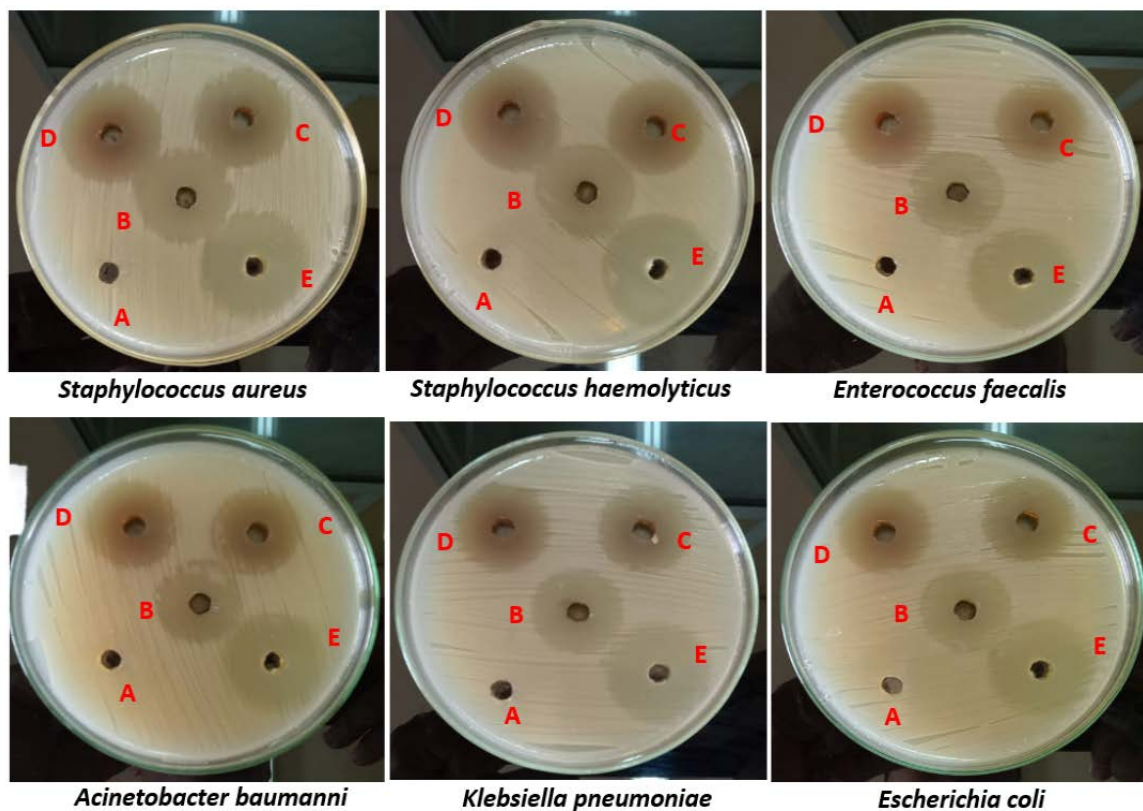


**Figure 5.** Anti-biofilm activity of (A) SCLe, (B) SCLe@MnO<sub>2</sub>NPs, and (C) CSH/SCLe@MnO<sub>2</sub>NPs against selected isolated bacteria pathogen's.

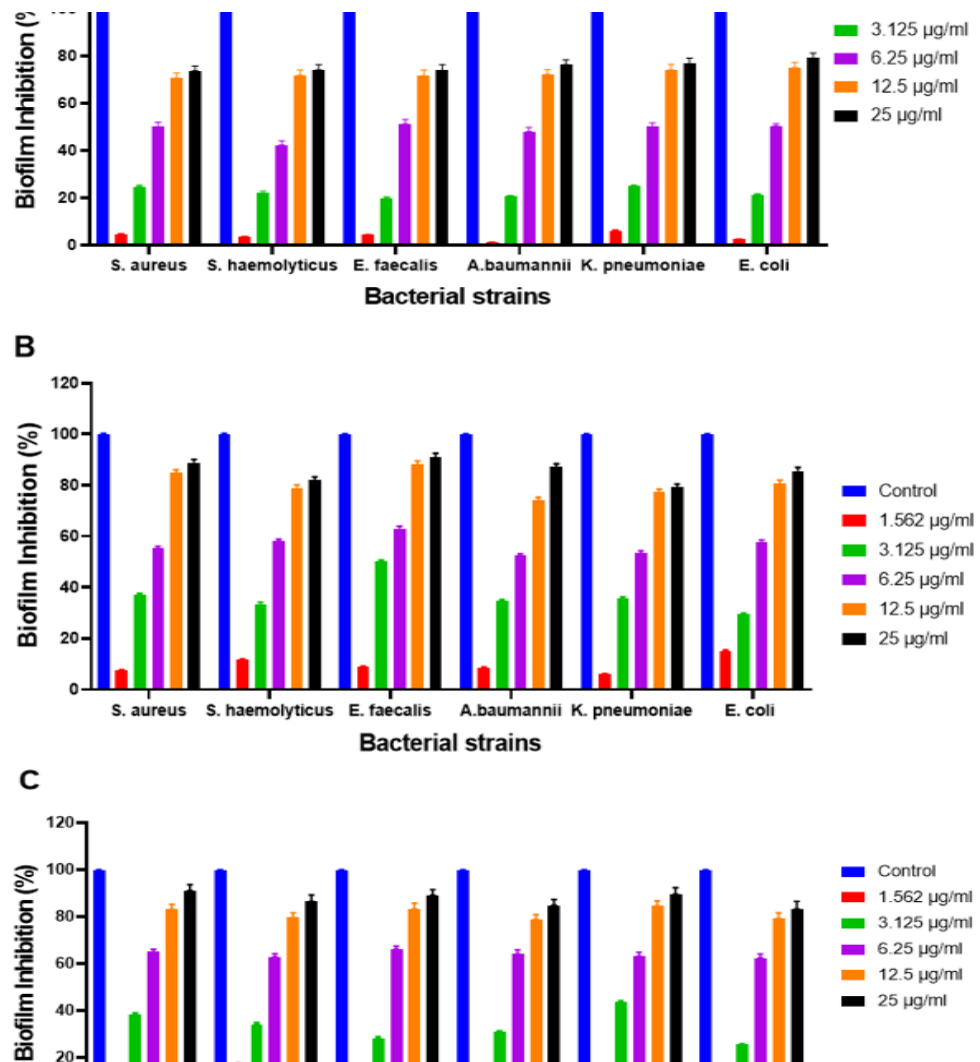
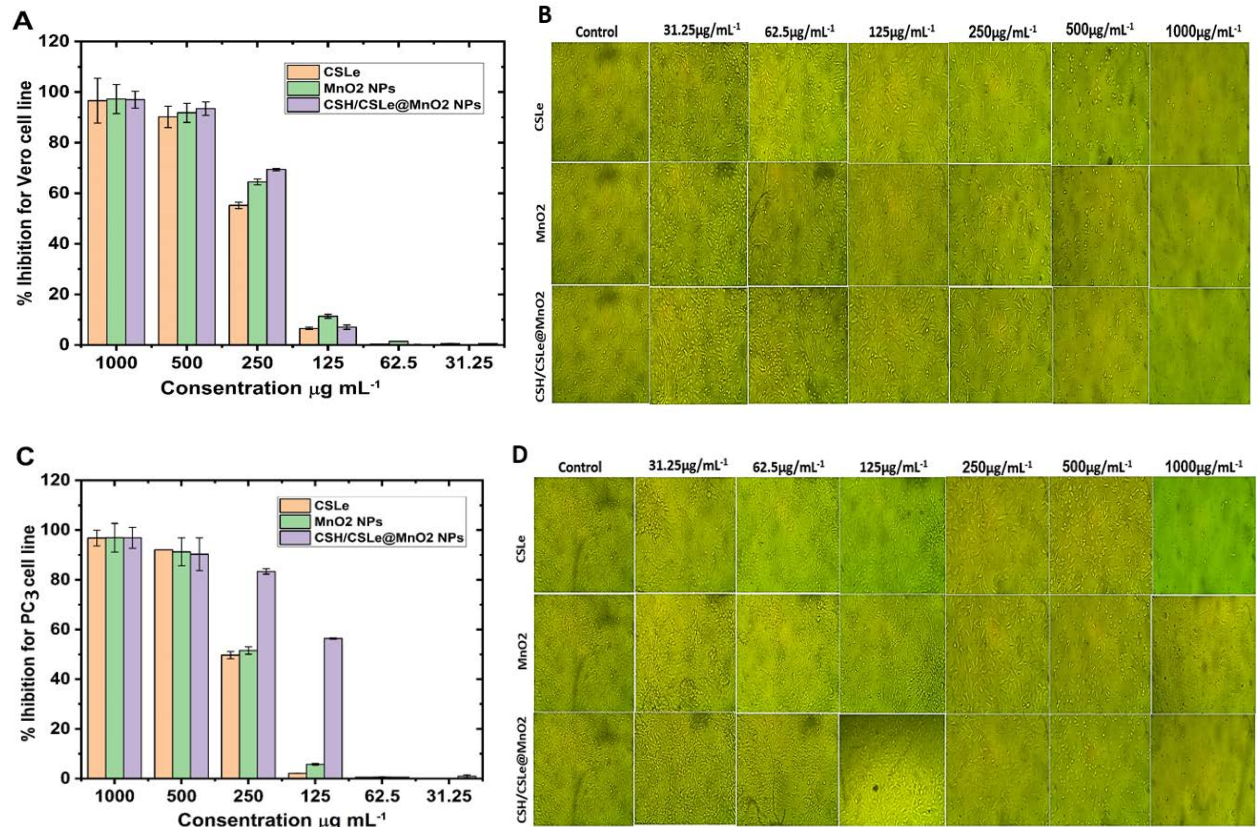




**Figure 6.** Cytotoxicity of SCLe, MnO<sub>2</sub> NPs, and CSH/SCLe@ MnO<sub>2</sub>NPs on normal Vero cells (A and B), and prostate carcinoma PC3 cells (C and D) for 24 h. The results were taken from replicated (*n*=3) (Mean ± SD). (B and D) Morphological features, the images were taken from the cells were treated with an average size of 10 nm for 24 h.



## ТИТУЛЬНЫЙ ЛИСТ\_МЕТАДААННЫЕ

### **Блок 1. Информация об авторе ответственном за переписку**

**Mohamed Elharrif** – (PhD) Department of Basic Medical Sciences, College of Medicine, Shaqra University, Shaqra 11961, Saudi Arabia;

telephone: +96656364746;

e-mail: al\_harrif@yahoo.com

### **Блок 2. Информация об авторах**

**Nasser Abdelhamid Hassan** – (PhD) Synthetic Unit, Department of Photochemistry, Chemical Industries Research Institute, National Research Centre, Cairo 12622, Egypt;

telephone: +201064058602;

e-mail: nasserabdelhamid@hotmail.com

**Mohamed Sharaf** – (PhD) Department of Biochemistry and Molecular Biology, College of Marine Life Sciences, Ocean University of China, Qingdao, 266003, China;

telephone: +201007775325;

e-mail: mohamedkamel@azhar.edu.eg

**Блок 1. Информация об авторе ответственном за переписку**

**Мохамед Элхарриф** – (к.н.) Кафедра фундаментальных медицинских наук,  
Медицинский колледж, Университет Шакры, Шакра 11961, Саудовская  
Аравия;

Телефон: +96656364746;

Электронная почта: al\_harrif@yahoo.com

**Блок 2. Информация об авторах**

**Насер Абдельхамид Хасан** – (к.н.) Отдел синтеза, кафедра фотохимии,  
Научно-исследовательский институт химической промышленности,  
Национальный исследовательский центр, Каир 12622, Египет;

Телефон: +201064058602;

Электронная почта: nasserabdelhamid@hotmail.com

**Мохамед Шараф** – (к.н.) Кафедра биохимии и молекулярной биологии,  
Колледж наук о морской жизни, Океанский университет Китая, Циндао,  
266003, Китай;

Телефон: +201007775325;

Электронная почта: mohamedkamel@azhar.edu.eg

**Блок 3. Метаданные статьи**

BIOSYNTHESIS OF NOVEL  $MnO_2$  NANOCAPSULES VIA *C. SPINOSA* EXTRACT AND HONEYBEE-DERIVED CHITOSAN: EXPLORING ANTIBACTERIAL AND ANTICANCER PROPERTIES

БИОСИНТЕЗ НОВЫХ НАНОКАПСУЛ  $MnO_2$  С ПОМОЩЬЮ ЭКСТРАКТА *C. SPINOSA* И ХИТОЗАНА МЕДОНОСНОЙ ПЧЕЛЫ: ИЗУЧЕНИЕ АНТИБАКТЕРИАЛЬНЫХ И ПРОТИВОРАКОВЫХ СВОЙСТВ

**Сокращенное название статьи для верхнего колонтитула:**

THERAPEUTIC PROPERTIES OF  $MnO_2$  NANOCAPSULES COPEDED HONEYBEES CHITOSAN

ТЕРАПЕВТИЧЕСКИЕ СВОЙСТВА НАНОКАПСУЛ  $MnO_2$  С ХИТОЗАНОМ МЕДОНОСНОЙ ПЧЕЛЫ

**Keywords:** *C. spinosa*,  $MnO_2$ NPs, Honeybees chitosan, Antibacterial, Anti-biofilm, Anticancer.

**Ключевые слова:** *C. spinosa*,  $MnO_2$ nps, хитозан медоносной пчелы, антибактериальные, антибиопленка, противораковые.

Оригинальные статьи.

Количество страниц текста – 23, количество таблиц – 2, количество рисунков – 6.

29.01.2024





## СПИСОК ЛИТЕРАТУРЫ

N O	Reference	URL
1	Abd-ElGawad, A. M., Y. A. El-Amier, A. M. Assaeed and S. L. J. S. J. o. B. S. Al-Rowaily (2020). "Interspecific variations in the habitats of <i>Reichardia tingitana</i> (L.) Roth leading to changes in its bioactive constituents and allelopathic activity. <i>Saudi J Biol Sci.</i> <b>27</b> (1): 489-499.	DOI: <a href="https://doi.org/10.1016/j.sjbs.2019.11.015">10.1016/j.sjbs.2019.11.015</a>
2	Abd Elgadir, M., M. S. Uddin, S. Ferdosh, A. Adam, A. J. K. Chowdhury, M. Z. I. J. J. o. f. Sarker and d. analysis (2015). "Impact of chitosan composites and chitosan nanoparticle composites on various drug delivery systems: A review." <i>Journal of Food and Drug Analysis</i> <b>23</b> (4): 619-629	DOI: <a href="https://doi.org/10.1016/j.jfda.2014.10.008">10.1016/j.jfda.2014.10.008</a>
3	Alqahtani, A. S., F. A. Nasr, M. Z. Ahmed, M. Y. Bin Mansour, A. A. Biksmawi, O. M. Noman, R. N. Herqash, M. Al-zharani, A. A. Qurtam and H. A. J. O. C. Rudayni (2023). "In vitro protective and anti-inflammatory effects of <i>Capparis spinosa</i> and its flavonoids profile." <i>Open Chemistry</i> <b>21</b> (1): 20230186.	<a href="https://doi.org/10.1515/chem-2023-0186">doi.org/10.1515/chem-2023-0186</a>
4	Alshawwa, S. Z., E. J. Mohammed, N. Hashim, M. Sharaf, S. Selim, H. M. Alhuthali, H. A. Alzahrani, A. E. Mekky and M. G. Elharrif (2022). "In Situ Biosynthesis of Reduced	DOI: <a href="https://doi.org/10.3390/antibiotics11091252">10.3390/antibiotics11091252</a>

	Alpha Hematite ( $\alpha$ -Fe <sub>2</sub> O <sub>3</sub> ) Nanoparticles by Stevia Rebaudiana L. Leaf Extract: Insights into Antioxidant, Antimicrobial, and Anticancer Properties." <i>Antibiotics</i> <b>11</b> (9): 1252.	
5	Arif, M., M. Sharaf, Samreen, S. Khan, Z. Chi and C.-G. Liu (2021). "Chitosan-based nanoparticles as delivery-carrier for promising antimicrobial glycolipid biosurfactant to improve the eradication rate of Helicobacter pylori biofilm." <i>Journal of Biomaterials Science, Polymer Edition</i> <b>32</b> (6): 813-832.	DOI: <a href="https://doi.org/10.1080/09205063.2020.1870323">10.1080/09205063.2020.1870323</a>
6	Azhir, E., R. Etefagh, M. Mashreghi and P. J. P. C. R. Pordeli (2015). "Preparation, characterization and antibacterial activity of manganese oxide nanoparticles." <i>Physical Chemistry Research</i> <b>3</b> (3): 197-204.	DOI: <a href="https://doi.org/10.22036/pcr.2015.9329">10.22036/pcr.2015.9329</a>
7	Bakour, M., M. d. G. Campos, H. Imtara and B. J. J. o. A. R. Lyoussi (2020). "Antioxidant content and identification of phenolic/flavonoid compounds in the pollen of fourteen plants using HPLC-DAD." <i>Journal of Apicultural Research</i> <b>59</b> (1): 35-41.	DOI: <a href="https://doi.org/10.1080/00218839.2019.1675336">10.1080/00218839.2019.1675336</a>
8	Bilal, M., Y. Zhao, T. Rasheed, I. Ahmed, S. T. Hassan, M. Z. Nawaz, H. M. J. I. j. o. e. r. Iqbal and p. health (2019). "Biogenic nanoparticle–chitosan conjugates with antimicrobial, antibiofilm, and anticancer potentialities: development and characterization." <i>Int. J. Environ. Res. Public Health</i> <b>16</b> (4): 598.	DOI: <a href="https://doi.org/10.3390/ijerph16040598">10.3390/ijerph16040598</a>

9	Ceriello, A. J. D. (2005). "Postprandial hyperglycemia and diabetes complications: is it time to treat?" <i>Diabetes</i> . <b>54</b> (1): 1-7.	DOI: <a href="https://doi.org/10.2337/diabetes.54.1.1">10.2337/diabetes.54.1.1</a>
10	Chandrasekaran, R., S. Gnanasekar, P. Seetharaman, R. Keppanan, W. Arockiaswamy and S. J. J. o. M. L. Sivaperumal (2016). "Formulation of Carica papaya latex-functionalized silver nanoparticles for its improved antibacterial and anticancer applications." <i>Journal of Molecular Liquids</i> <b>219</b> : 232-238.	<a href="https://doi.org/10.1016/j.molliq.2016.03.038">https://doi.org/10.1016/j.molliq.2016.03.038</a>
11	Cushnie, T. T. and A. J. Lamb (2005). "Antimicrobial activity of flavonoids." <i>International journal of antimicrobial agents</i> <b>26</b> (5): 343-356.	DOI: <a href="https://doi.org/10.1016/j.ijantimicag.2005.09.002">10.1016/j.ijantimicag.2005.09.002</a>
12	Danaei, M., M. Dehghankhold, S. Ataei, F. Hasanzadeh Davarani, R. Javanmard, A. Dokhani, S. Khorasani and M. Mozafari (2018). "Impact of particle size and polydispersity index on the clinical applications of lipidic nanocarrier systems." <i>Pharmaceutics</i> <b>10</b> (2): 57.	<a href="https://doi.org/10.3390/pharmaceutics10020057">10.3390/pharmaceutics10020057</a>
13	Dang, T.-D., M. A. Cheney, S. Qian, S. W. Joo, B.-K. J. I. Min and E. C. Research (2013). "A novel rapid one-step synthesis of manganese oxide nanoparticles at room temperature using poly (dimethylsiloxane)." <i>Ind. Eng. Chem. Res.</i> <b>52</b> (7): 2750-2753.	<a href="https://doi.org/10.1021/ie302971g">https://doi.org/10.1021/ie302971g</a>
14	Eaton, P., J. C. Fernandes, E. Pereira, M. E. Pintado and F. X. Malcata (2008). "Atomic	DOI: <a href="https://doi.org/10.1016/j.ultramic.2008.03.002">10.1016/j.ultramic.2008.03.002</a>

	force microscopy study of the antibacterial effects of chitosans on Escherichia coli and Staphylococcus aureus." <u>Ultramicroscopy</u> <b>108</b> (10): 1128-1134.	<a href="#">8.04.015</a>
15	El Rabey, H. A., F. M. Almutairi, A. I. Alalawy, M. A. Al-Duais, M. I. Sakran, N. S. Zidan and A. A. Tayel (2019). "Augmented control of drug-resistant Candida spp. via fluconazole loading into fungal chitosan nanoparticles." <u>International Journal of Biological Macromolecules</u> <b>141</b> : 511-516.	DOI: <a href="#">10.1016/j.ijbiomac.2019.09.036</a>
16	Elnosary, M. E., H. A. Aboelmagd, M. A. Habaka, S. R. Salem and M. E. El-Naggar (2023). "Synthesis of bee venom loaded chitosan nanoparticles for anti-MERS-COV and multi-drug resistance bacteria." <u>International Journal of Biological Macromolecules</u> <b>224</b> : 871-880	doi: <a href="#">10.1016/j.ijbiomac.2022.10.173</a>
17	Fu, P. P., Q. Xia, H.-M. Hwang, P. C. Ray and H. Yu (2014). "Mechanisms of nanotoxicity: generation of reactive oxygen species." <u>Journal of food and drug analysis</u> <b>22</b> (1): 64-75.	DOI: <a href="#">10.1016/j.jfda.2014.01.005</a>
18	Gan, Q. and T. Wang (2007). "Chitosan nanoparticle as protein delivery carrier—systematic examination of fabrication conditions for efficient loading and release." <u>Colloids and Surfaces B: Biointerfaces</u> <b>59</b> (1): 24-34	<a href="https://doi.org/10.1016/j.colsurfb.2007.04.009">https://doi.org/10.1016/j.colsurfb.2007.04.009</a>
19	Ganesh, P. S. and V. R. Rai (2018). "Attenuation of quorum-sensing-dependent virulence	doi: <a href="#">10.1016/j.jtcme.2017.05.</a>

	factors and biofilm formation by medicinal plants against antibiotic resistant <i>Pseudomonas aeruginosa</i> ." <u>Journal of traditional and complementary medicine</u> <b>8</b> (1): 170-177.	<a href="#">008</a>
20	Harrigan, W. F. and M. E. McCance (1976). <u>Laboratory methods in food and dairy microbiology</u> , Academic Press Inc.(London) Ltd.	
21	Haydarova, X. and G. Ikhtiyarova (2019). "Method of obtaining a chitosan aminopolisaccharide from behbat <i>Apis Mellifera</i> ." <u>Journal of chemistry Kazakhstan</u> (2): 69-74.	<a href="https://chemjournal.kz/index.php/journal/article/view/179">https://chemjournal.kz/index.php/journal/article/view/179</a>
22	Hoseinpour, V. and N. J. M. R. E. Ghaemi (2018). "Novel ZnO–MnO <sub>2</sub> –Cu <sub>2</sub> O triple nanocomposite: facial synthesis, characterization, antibacterial activity and visible light photocatalytic performance for dyes degradation-A comparative study." <u>Materials Research Express</u> <b>5</b> (8): 085012.	<a href="https://api.semanticscholar.org/CorpusID:105445929">https://api.semanticscholar.org/CorpusID:105445929</a>
23	Ingale, A. G. and A. J. J. N. N. Chaudhari (2013). "Biogenic synthesis of nanoparticles and potential applications: an eco-friendly approach." <u>J Nanomed Nanotechol</u> <b>4</b> (165): 1-7.	DOI: 10.4172/2157-7439.1000165
24	Jaganyi, D., M. Altaf and I. J. A. N. Wekesa (2013). "Synthesis and characterization of	DOI:

	whisker-shaped MnO <sub>2</sub> nanostructure at room temperature." <i>Appl Nanosci</i> <b>3</b> : 329-333	<a href="https://doi.org/10.1007/s13204-012-0135-3">https://doi.org/10.1007/s13204-012-0135-3</a>
25	Jayandran, M., M. M. Haneefa and V. J. J. o. A. P. S. Balasubramanian (2015). "Green synthesis and characterization of Manganese nanoparticles using natural plant extracts and its evaluation of antimicrobial activity." <i>Journal of Applied Pharmaceutical Science</i> <b>5</b> (12): 105-110.	DOI: <a href="https://doi.org/10.7324/JAPS.2015.501218">10.7324/JAPS.2015.501218</a>
26	Jeyaraj, M., G. Sathishkumar, G. Sivanandhan, D. MubarakAli, M. Rajesh, R. Arun, G. Kapildev, M. Manickavasagam, N. Thajuddin, K. J. C. Premkumar and s. B. Biointerfaces (2013). "Biogenic silver nanoparticles for cancer treatment: an experimental report." <i>Colloids Surf B Biointerfaces</i> . <b>106</b> : 86-92.	DOI: <a href="https://doi.org/10.1016/j.colsurfb.2013.01.027">10.1016/j.colsurfb.2013.01.027</a>
27	Joshi, N. C., E. Joshi, A. J. R. J. o. P. Singh and Technology (2020). "Biological Synthesis, Characterisations and Antimicrobial activities of manganese dioxide (MnO <sub>2</sub> ) nanoparticles." <i>Research J. Pharm. and Tech</i> <b>13</b> (1): 135-140.	DOI: <a href="https://doi.org/10.5958/0974-360X.2020.00027.X">10.5958/0974-360X.2020.00027.X</a>
28	Joshi, N. C., F. Siddiqui, M. Salman and A. J. A. P. J. H. S. Singh (2020). "Antibacterial activity, characterizations, and biological synthesis of manganese oxide nanoparticles using the extract of aloe vera." <i>Asian Pacific Journal of Health Sciences</i> <b>7</b> : 27-29.	<b>DOI:</b> <a href="https://doi.org/10.21276/apjhs.2020.7.3.7">https://doi.org/10.21276/apjhs.2020.7.3.7</a>
29	Kant, R., S. Pathak, V. J. S. E. M. Dutta and S. Cells (2018). "Design and fabrication of	DIO:

	sandwich-structured $\alpha$ -Fe <sub>2</sub> O <sub>3</sub> /Au/ZnO photoanode for photoelectrochemical water splitting." <i>Solar Energy Materials and Solar Cells</i> <b>178</b> : 38-45.	<a href="https://doi.org/10.1016/j.solmat.2018.01.005">https://doi.org/10.1016/j.solmat.2018.01.005</a>
30	Khan, S. A., S. Shahid, B. Shahid, U. Fatima and S. A. J. B. Abbasi (2020). "Green synthesis of MnO nanoparticles using abutilon indicum leaf extract for biological, photocatalytic, and adsorption activities." <i>Biomolecules</i> <b>10</b> (5): 785.	doi: <a href="https://doi.org/10.3390/biom10050785">10.3390/biom10050785</a>
31	Khanna, P., C. Ong, B. H. Bay and G. H. Baeg (2015). "Nanotoxicity: an interplay of oxidative stress, inflammation and cell death." <i>Nanomaterials</i> <b>5</b> (3): 1163-1180.	doi: <a href="https://doi.org/10.3390/nano5031163">10.3390/nano5031163</a>
32	Khomsii, M. E., H. Imtara, M. Kara, A. Hmamou, A. Assouguem, B. Bourkhiss, M. Tarayrah, M. N. AlZain, N. M. Alzamel and O. J. M. Noman (2022). "Antimicrobial and antioxidant properties of total polyphenols of <i>Anchusa italica</i> Retz." <i>Molecules</i> . <b>27</b> (2): 416.	DOI: <a href="https://doi.org/10.3390/molecules27020416">10.3390/molecules27020416</a>
33	Kravanja, G., M. Primožič, Ž. Knez and M. J. M. Leitgeb (2019). "Chitosan-based (Nano) materials for novel biomedical applications." <i>Molecule</i> . <b>24</b> (10): 1960.	DOI: <a href="https://doi.org/10.3390/molecules24101960">10.3390/molecules24101960</a>
34	Kulkarni, A., A. Srivastava, R. Nagalgaon and R. J. I. J. B. P. R. Zunjarrao (2012). "Phytofabrication of silver nanoparticles from a novel plant source and its application." <b>3</b> (3): 417-421.	
35	Kumar, G. S., B. Venkataramana, S. A. Reddy, H. Maseed, R. R. J. A. i. N. S. N.	DOI: <a href="https://doi.org/10.1088/2043-">10.1088/2043-</a>



	Nagireddy and Nanotechnology (2020). "Hydrothermal synthesis of Mn <sub>3</sub> O <sub>4</sub> nanoparticles by evaluation of pH effect on particle size formation and its antibacterial activity." <i>Advances in Natural Sciences Nanoscience and Nanotechnology</i> <b>11</b> (3): 035006.	<a href="https://doi.org/10.15789/2220-7619-BON-17582">6254/ab9cac</a>
36	Kunkalekar, R. (2019). Role of oxides (Fe <sub>3</sub> O <sub>4</sub> , MnO <sub>2</sub> ) in the antibacterial action of Ag–metal oxide hybrid nanoparticles. <i>Noble Metal-Metal Oxide Hybrid Nanoparticles</i> , Elsevier: 303-312.	<a href="https://doi.org/10.1016/B978-0-12-814134-2.00010-3">https://doi.org/10.1016/B978-0-12-814134-2.00010-3</a>
37	Li, Y., J. Liu, L. Wang, J. Zhang, Z. Wang, Z. Gao, Y. Zhong and D. Zhang (2011). <u>Notice of Retraction: Preparation and Characterization of Mn<sub>0.5</sub>Zn<sub>0.5</sub>Fe<sub>2</sub>O<sub>4</sub>@ Au Composite Nanoparticles and Its Anti-Tumor Effect on Hepatocellular Carcinoma Cells.</u> 2011 5th International Conference on Bioinformatics and Biomedical Engineering, IEEE.	<b>DOI:</b> <a href="https://doi.org/10.1109/icbbe.2011.5781653">10.1109/icbbe.2011.5781653</a>
38	Lotfy, V. F. and A. H. Basta (2022). "A green approach to the valorization of kraft lignin for the production of nanocomposite gels to control the release of fertilizer." <i>Biofuels, Bioproducts and Biorefining</i> <b>16</b> (2): 488-498.	DOI: <a href="https://doi.org/10.1002/bbb.2317">https://doi.org/10.1002/bbb.2317</a>
39	Lu, H., X. Zhang, S. A. Khan, W. Li and L. J. F. i. m. Wan (2021). "Biogenic synthesis of MnO <sub>2</sub> nanoparticles with leaf extract of <i>Viola betonicifolia</i> for enhanced antioxidant, antimicrobial, cytotoxic, and biocompatible applications." <i>Front. Microbio</i> <b>12</b> : 761084.	<a href="https://doi.org/10.3389/fmicb.2021.761084">https://doi.org/10.3389/fmicb.2021.761084</a>
40	Majani, S. S., S. Sathyan, M. V. Manoj, N. Vinod, S. Pradeep, C. Shivamallu, K.	<a href="https://doi.org/10.1016/j.crgs">https://doi.org/10.1016/j.crgs</a>

	Venkatachalaiah, S. P. J. C. R. i. G. Kollur and S. Chemistry (2023). "Eco-friendly synthesis of MnO <sub>2</sub> nanoparticles using Saraca asoca leaf extract and evaluation of in vitro anticancer activity." <i>Current Research in Green and Sustainable Chemistry</i> 100367.	<a href="https://doi.org/10.15789/2023/100367">с.2023.100367</a>
41	Manjula, R., M. Thenmozhi, S. Thilagavathi, R. Srinivasan and A. J. M. T. P. Kathirvel (2020). "Green synthesis and characterization of manganese oxide nanoparticles from Gardenia resinifera leaves." <i>Materials Today: Proceedings</i> <b>26</b> : 3559-3563.	doi: <a href="https://doi.org/10.1155/2013/942916">10.1155/2013/942916</a>
42	Manke, A., L. Wang and Y. Rojanasakul (2013). "Mechanisms of nanoparticle-induced oxidative stress and toxicity." <i>BioMed research international</i> <b>2013</b> .	<a href="https://doi.org/10.1016/j.matpr.2019.07.396">https://doi.org/10.1016/j.matpr.2019.07.396</a>
43	Marchand, G., G. Fabre, N. Maldonado-Carmona, N. Villandier and S. Leroy-Lhez (2020). "Acetylated lignin nanoparticles as a possible vehicle for photosensitizing molecules." <i>Nanoscale Advances</i> <b>2</b> (12): 5648-5658.	<b>DOI</b> <a href="https://doi.org/10.1039/D0N1A00615G">https://doi.org/10.1039/D0N1A00615G</a>
44	Mohamed, D. I., D. Alaa El-Din Aly El-Waseef, E. S. Nabih, O. A. El-Kharashi, H. F. Abd El-Kareem, H. H. Abo Nahas, B. A. Abdel-Wahab, Y. A. Helmy, S. Z. Alshawwa and E. M. J. P. Saied (2022). "Acetylsalicylic acid suppresses alcoholism-induced cognitive impairment associated with atorvastatin intake by targeting cerebral MiRNA155 and NLRP3: In vivo, and in silico study." <b>14</b> (3): 529.	DOI: <a href="https://doi.org/10.3390/ph15070832">10.3390/ph15070832</a>
45	Mohamed, D. I., S. F. Ezzat, W. M. Elayat, O. A. El-Kharashi, H. F. A. El-Kareem, H. H.	DOI: <a href="https://doi.org/10.3390/ph15070832">10.3390/ph15070832</a>

	A. Nahas, B. A. Abdel-Wahab, S. Z. Alshawwa, A. Saleh and Y. A. J. P. Helmy (2022). "Hepatoprotective role of carvedilol against ischemic hepatitis associated with acute heart failure via targeting MiRNA-17 and mitochondrial dynamics-related proteins: An in vivo and in silico study." <i>Pharmaceuticals (Basel)</i> <b>15</b> (7): 832.	
46	Moon, S. A., B. K. Salunke, B. Alkotaini, E. Sathiyamoorthi and B. S. J. I. n. Kim (2015). "Biological synthesis of manganese dioxide nanoparticles by <i>Kalopanax pictus</i> plant extract." <i>IET Nanobiotechnol</i> <b>9</b> (4): 220-225.	DOI: <a href="https://doi.org/10.1049/iet-nbt.2014.0051">10.1049/iet-nbt.2014.0051</a>
47	Morena, A. G., I. Stefanov, K. Ivanova, S. I. Pérez-Rafael, M. Sánchez-Soto and T. Tzanov (2020). "Antibacterial polyurethane foams with incorporated lignin-capped silver nanoparticles for chronic wound treatment." <i>Industrial &amp; Engineering Chemistry Research</i> <b>59</b> (10): 4504-4514.	DOI: <a href="https://doi.org/10.1021/acs.iecr.9b06362">10.1021/acs.iecr.9b06362</a>
48	Neamah, S. A., S. Albukhaty, I. Q. Falih, Y. H. Dewir and H. B. J. A. S. Mahood (2023). "Biosynthesis of Zinc Oxide Nanoparticles Using <i>Capparis spinosa</i> L. Fruit Extract: Characterization, Biocompatibility, and Antioxidant Activity." <i>Appl. Sci.</i> <b>13</b> (11): 6604.	<a href="https://doi.org/10.1016/B978-0-12-822446-5.00010-1">https://doi.org/10.1016/B978-0-12-822446-5.00010-1</a>
49	Özçelik, B., D. D. Orhan, S. Özgen and F. Ergun (2008). "Antimicrobial activity of flavonoids against extended-spectrum $\beta$ -lactamase (ES $\beta$ L)-producing <i>Klebsiella pneumoniae</i> ." <i>Tropical Journal of Pharmaceutical Research</i> <b>7</b> (4): 1151-1157.	DOI: <a href="https://doi.org/10.4314/tjpr.v7i4.14701">10.4314/tjpr.v7i4.14701</a>

50	Pagar, T., S. Ghotekar, K. Pagar, S. Pansambal and R. Oza (2021). Phytogetic synthesis of manganese dioxide nanoparticles using plant extracts and their biological application. <u>Handbook of greener synthesis of nanomaterials and compounds</u> , Elsevier: 209-218.	<a href="https://doi.org/10.3390/app13116604">https://doi.org/10.3390/app13116604</a>
51	Piao, M. J., K. A. Kang, I. K. Lee, H. S. Kim, S. Kim, J. Y. Choi, J. Choi and J. W. J. T. I. Hyun (2011). "Silver nanoparticles induce oxidative cell damage in human liver cells through inhibition of reduced glutathione and induction of mitochondria-involved apoptosis." <i>Toxicol Lett</i> . <b>201</b> (1): 92-100.	DOI: <a href="https://doi.org/10.1016/j.toxlet.2010.12.010">10.1016/j.toxlet.2010.12.010</a>
52	Procop, G. W., D. L. Church, G. S. Hall and W. M. Janda (2020). <u>Koneman's color atlas and textbook of diagnostic microbiology</u> , Jones & Bartlett Publishers.	
53	Qi, L.-F., Z.-R. Xu, Y. Li, X. Jiang and X.-Y. J. W. J. o. G. W. Han (2005). "In vitro effects of chitosan nanoparticles on proliferation of human gastric carcinoma cell line MGC803 cells." <i>World J Gastroenterol</i> <b>11</b> (33): 5136.	doi: <a href="https://doi.org/10.3748/wjg.v11.i33.5136">10.3748/wjg.v11.i33.5136</a>
54	Raza, M. A., F. Mukhtar and M. Danish (2015). "Cuscuta reflexa and Carthamus Oxyacantha: potent sources of alternative and complimentary drug." <i>Springerplus</i> <b>4</b> (1): 1-6.	DOI: <a href="https://doi.org/10.1186/s40064-015-0854-5">10.1186/s40064-015-0854-5</a>
55	Razanamahandry, L. C., C. Onwordi, W. Saban, A. Bashir, L. Mekuto, E. Malenga, E. Manikandan, E. Fosso-Kankeu, M. Maaza and S. K. O. J. J. o. H. M. Ntwampe (2019).	<a href="https://doi.org/10.1016/j.jhazmat.2019.120900">https://doi.org/10.1016/j.jhazmat.2019.120900</a>

	"Performance of various cyanide degrading bacteria on the biodegradation of free cyanide in water." <i>Journal of Hazardous Materials</i> <b>380</b> : 120900.	
56	Rios, J.-L. and M. C. Recio (2005). "Medicinal plants and antimicrobial activity." <i>Journal of ethnopharmacology</i> <b>100</b> (1-2): 80-84.	DOI: 10.1016/j.jep.2005.04.025
57	Saad, W. M., L. L. Hamid, N. J. Alaallah and A. J. B. R. Ramizy (2022). "Biosynthesis and antibacterial activity of manganese oxide nanoparticles prepared by green tea extract." <i>Biotechnology Reports</i> <b>34</b> : e00729.	<a href="https://doi.org/10.1016/j.btrec.2022.e00729">https://doi.org/10.1016/j.btrec.2022.e00729</a>
58	Selim, M. S., N. A. Fathallah, S. A. Higazy, X. Chen, Z. J. M. C. Hao and Physics (2023). "Novel blade-like structure of reduced graphene oxide/ $\alpha$ -Mn <sub>2</sub> O <sub>3</sub> nanocomposite as an antimicrobial active agent against aerobic and anaerobic bacteria." <i>Materials Chemistry and Physics</i> <b>298</b> : 127436.	<a href="https://doi.org/10.1016/j.matchemphys.2023.127436">https://doi.org/10.1016/j.matchemphys.2023.127436</a>
59	Selim, M. S., H. Hamouda, Z. Hao, S. Shabana and X. Chen (2020). "Design of $\gamma$ -AlOOH, $\gamma$ -MnOOH, and $\alpha$ -Mn <sub>2</sub> O <sub>3</sub> nanorods as advanced antibacterial active agents." <i>Dalton Transactions</i> <b>49</b> (25): 8601-8613.	<a href="https://doi.org/10.1039/D0DT01689F">https://doi.org/10.1039/D0DT01689F</a>
60	Severino, R., G. Ferrari, K. D. Vu, F. Donsi, S. Salmieri and M. J. F. c. Lacroix (2015). "Antimicrobial effects of modified chitosan based coating containing nanoemulsion of essential oils, modified atmosphere packaging and gamma irradiation against Escherichia	<a href="https://doi.org/10.1016/j.foodcont.2014.08.029">https://doi.org/10.1016/j.foodcont.2014.08.029</a>

	coli O157: H7 and Salmonella Typhimurium on green beans." Food Control <b>50</b> : 215-222.	
61	Shahid, S. A., F. Anwar, M. Shahid, N. Majeed, A. Azam, M. Bashir, M. Amin, Z. Mahmood and I. J. J. o. N. Shakir (2015). "Laser-Assisted synthesis of Mn 0.50 Zn 0.50 Fe 2 O 4 nanomaterial: characterization and in vitro inhibition activity towards bacillus subtilis biofilm." Journal of Nanomaterials <b>16</b> (1): 111-111	<a href="https://doi.org/10.1155/2015/896185">https://doi.org/10.1155/2015/896185</a>
62	Sharaf, M., A. H. Sewid, H. Hamouda, M. G. Elharrif, A. S. El-Demerdash, A. Alharthi, N. Hashim, A. A. Hamad, S. Selim and D. H. M. Alkhalifah (2022). "Rhamnolipid-coated iron oxide nanoparticles as a novel multitarget candidate against major foodborne e. coli serotypes and methicillin-resistant s. aureus." <u>Microbiology Spectrum</u> <b>10</b> (4): e00250-00222.	DOI: 10.1128/spectrum.00250-22
63	Sharma, G., A. Kumar, M. Naushad, A. García-Peñas, H. Ala'a, A. A. Ghfar, V. Sharma, T. Ahamad and F. J. J. C. p. Stadler (2018). "Fabrication and characterization of Gum arabic-cl-poly (acrylamide) nanohydrogel for effective adsorption of crystal violet dye." Carbohydrate Polymers <b>202</b> : 444-453.	<a href="https://doi.org/10.1016/j.carbpol.2018.09.004">https://doi.org/10.1016/j.carbpol.2018.09.004</a>
64	Silva, L. P. d., D. de Britto, M. H. R. Selegim and O. B. Assis (2010). "In vitro activity of water-soluble quaternary chitosan chloride salt against E. coli." <u>World Journal of Microbiology and Biotechnology</u> <b>26</b> (11): 2089-2092.	<a href="https://doi.org/10.1007/s11274-010-0378-7">https://doi.org/10.1007/s11274-010-0378-7</a>

65	Souri, M., V. Hoseinpour, A. Shakeri and N. J. I. n. Ghaemi (2018). "Optimisation of green synthesis of MnO nanoparticles via utilising response surface methodology." IET Nanobiotechnol <b>12</b> (6): 822-827.	doi: 10.1049/iet-nbt.2017.0145
66	Srinivasa, C., S. S. Kumar, S. Pradeep, S. K. Prasad, R. Veerapur, M. A. Ansari, M. N. Alomary, S. Alghamdi, M. Almeahmadi and K. J. I. J. o. N. Gc (2022). "Eco-friendly synthesis of MnO <sub>2</sub> nanorods using gmelina arborea fruit extract and its anticancer potency against MCF-7 breast cancer cell line." Int J Nanomedicine. 17: 901-907	DOI: 10.2147/IJN.S335848
67	Sun, S.-N., M.-F. Li, T.-Q. Yuan, F. Xu, R.-C. J. I. c. Sun and products (2013). "Effect of ionic liquid/organic solvent pretreatment on the enzymatic hydrolysis of corncob for bioethanol production. Part 1: Structural characterization of the lignins." Industrial Crops and Products <b>43</b> : 570-577.	<a href="https://doi.org/10.1016/j.indcrop.2012.07.074">https://doi.org/10.1016/j.indcrop.2012.07.074</a>
68	Suzuki, S. and M. J. N. Miyayama (2017). "Structural Distortion in MnO <sub>2</sub> Nanosheets and Its Suppression by Cobalt Substitution." Nanomaterials <b>7</b> (10): 295.	<a href="https://doi.org/10.3390/nano7100295">https://doi.org/10.3390/nano7100295</a>
69	Svirskaya, S. and A. Grytsyk (2018). "Investigation of tannins in <i>Anchusa officinalis</i> L." Pharma Innovation <b>7</b> (4):758-761.	
70	Taleb, F., M. Ammar, M. b. Mosbah, R. b. Salem and Y. Moussaoui (2020). "Chemical modification of lignin derived from spent coffee grounds for methylene blue adsorption." <a href="https://doi.org/10.1038/s4159">https://doi.org/10.1038/s4159</a>	

	<u>Scientific Reports</u> <b>10</b> (1): 1-13.	8-020-68047-6
71	Vashistha, V. K., S. Gautam, R. Bala, A. Kumar, D. K. J. R. Das and A. i. Chemistry (2022). "Transition Metal-Based Nanoparticles as Potential Antimicrobial Agents." <i>Discov Nano</i> <b>12</b> (4): 222-247.	DOI: 10.1186/s11671-023-03861-1
72	Xia, H.-Y., B.-Y. Li, Y. Zhao, Y.-H. Han, S.-B. Wang, A.-Z. Chen and R. K. J. C. C. R. Kankala (2022). "Nanoarchitected manganese dioxide (MnO <sub>2</sub> )-based assemblies for biomedicine." <i>Coordination Chemistry Reviews</i> <b>464</b> : 214540.	<a href="https://doi.org/10.1016/j.ccr.2022.214540">https://doi.org/10.1016/j.ccr.2022.214540</a>
73	Zhang HongXia, Z. H. and M. Z. Ma ZhengFeei (2018). "Phytochemical and pharmacological properties of <i>Capparis spinosa</i> as a medicinal plant." <i>Nutrients</i> . <b>10</b> (2):116.	doi: <a href="https://doi.org/10.3390/nu10020116">10.3390/nu10020116</a>